VILNIUS GEDIMINAS TECHNICAL UNIVERSITY

FACULTY OF ENVIROMENTAL ENGINEERING

DEPARTMENT OF ROADS

RIGA TECHNICAL UNIVERSITY

FACULTY OF CIVIL ENGINEERING

DEPARTMENT OF ROADS AND BRIDGES

AIDA MOUQUAFI

DEFLECTION INVESTIGATION OF CONCRETE BEAMS REINFORCED WITH STEEL BARS AND FIBRES

FINAL MASTER'S THESIS

INNOVATIVE ROAD AND BRIDGE ENGINEERING

study programme

state code 6281EX002

CIVIL ENGINEERING study field

VILNIUS, 2025

VILNIUS GEDIMINAS TECHNICAL UNIVERSITY

FACULTY OF ENVIROMENTAL ENGINEERING
DEPARTMENT OF ROADS

RIGA TECHNICAL UNIVERSITY

FACULTY OF CIVIL ENGINEERING
DEPARTMENT OF ROADS AND BRIDGES

APPROVED BY

Head of Department

_____

(Signature)

_____

(Name, Surname)

_____

(Date)

AIDA MOUQUAFI

DEFLECTION INVESTIGATION OF CONCRETE BEAMS REINFORCED WITH STEEL BARS AND FIBRES

FINAL MASTER'S THESIS

INNOVATIVE ROAD AND BRIDGE ENGINEERING study programme

state code 6281EX002

CIVIL ENGINEERING study field

Supervisor: Assoc. Prof. Dr. GINTARIS KAKLAUSKAS_____2025-01-06

(Title, Name, Surname) (Signature) (Date)

VILNIUS, 2025

VILNIUS GEDIMINAS TECHNICAL UNIVERSITY
FACULTY OF ENVIROMENTAL ENGINEERING
DEPARTMENT OF ROADS

RIGA TECHNICAL UNIVERSITY
FACULTY OF CIVIL ENGINEERING
DEPARTMENT OF ROADS AND BRIDGES

CIVIL ENGINEERING study field
INNOVATIVE ROAD AND BRIDGE ENGINEERING study programme
state code *6281EX002*

OBJECTIVES FOR MASTER THESIS
.....……...No. .....
Riga and Vilnius

For student: Aida Mouquafi

Master Thesis title: DEFLECTION INVESTIGATION OF CONCRETE BEAMS REINFORCED WITH STEEL BARS AND FIBRES

The master thesis has to be completed by: 06 January, 2025

THE OBJECTIVES:

1) To review the methods for deflection analysis of concrete beams reinforced with steel bars and fibers.
2) Collect experimental data from the literature on deflections of concrete beams reinforced with steel bars and fibers bars.
3) To examine the accuracy of the new curvature model for predicting deflection of reinforced concrete beams reinforced with steel bars and fibers bars.
4) To suggest some directions for future investigations.

Academic Supervisor (Signature) (GINTARIS KAKLAUSKAS)
(Title, Name, Surname)

Objectives accepted as a guidance for my Master Thesis

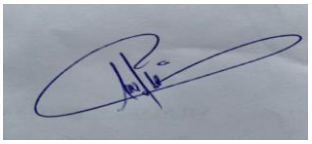

(Student‘s signature)
AIDA MOUQUAFI
(Student‘s Name, Surname)
2025-01-06
(Date)

VILNIUS GEDIMINAS TECHNICAL UNIVERSITY

Aida Mouquafi, 20233802

(Student's given name, family name, certificate number)

Faculty of Environmental Engineering

(Faculty)

Innovative Road and Bridge Engineering, IKTfmu-23

(Study programme, academic group no.)

DECLARATION OF AUTHORSHIP IN THE FINAL DEGREE PROJECT

January 6, 2025

I declare that my Final Degree Project entitled „Deflection Investigation of Concrete Beams Reinforced with Steel Bars and Fibres“ is entirely my own work. I have clearly signalled the presence of quoted or paraphrased material and referenced all sources.

I have acknowledged appropriately any assistance I have received by the following professionals/advisers: Prof Doctor Habilus Gintaris Kaklauskas.

The academic supervisor of my Final Degree Project is Prof Doctor Habilus Gintaris Kaklauskas.

No contribution of any other person was obtained, nor did I buy my Final Degree Project.

(Signature)

Aida Mouquafi

(Given name, family name)

VILNIAUS GEDIMINO TECHNIKOS UNIVERSITETAS
APLINKOS INŽINERIJOS FAKULTETAS
KELIŲ KATEDRA

Kalba:

Anglų

Anotacija

Betono sijų, armatuotų plieninėmis armatūromis ir pluoštais, defleksijos tyrimas nagrinėja pluoštų įtraukimo poveikį lenkimo elgsenai ir defleksijos reakcijai.
Tyrimas orientuojasi į sijų, armatuotų skirtingomis plieninės armatūros ir pluoštų kombinacijomis, palyginimą, siekiant įvertinti jų įtaką sijų defleksijai veikiant apkrovoms. Rezultatai rodo, kad pluoštų armatūra pagerina elgseną po įtrūkimų, sumažina įtrūkimų plotį ir gerina defleksijos kontrolę, palyginti su tradicine tik plienine armatūra.
Ypač plieniniai pluoštai suteikia geresnį atsparumą defleksijai, padidindami betono tempimo stiprumą ir kietumą. Tyrimo išvados rodo, kad pluoštų įtraukimas į armatuotus betoninius sijus gali pagerinti jų eksploatacines savybes ir ilgaamžiškumą, todėl tai yra perspektyvi sprendimo galimybė struktūriniams elementams, veikiantiems lenkimo ir dinaminėmis apkrovomis

VILNIUS GEDIMINAS TECHNICAL UNIVERSITY
FACULTY OF ENVIROMENTAL ENGINEERING
EPARTMENT OF ROADS

Thesis Language

Foreign (English)

Annotation

The deflection investigation of concrete beams reinforced with steel bars and fibers examines the impact of fiber inclusion on the bending behavior and deflection response of reinforced concrete beams.

The study focuses on comparing beams reinforced with different combinations of steel reinforcement and fibers, to assess their influence on beam deflection under applied loads.

Results show that fiber reinforcement enhances post-cracking behavior, reduces crack width, and improves deflection control compared to traditional steel-only reinforcement.

Steel fibers, in particular, are found to provide better deflection resistance by enhancing the tensile strength and toughness of the concrete.

The findings suggest that incorporating fibers in reinforced concrete beams can offer improved serviceability and durability, making them a viable solution for structural elements subject to bending and dynamic loads.

Vilnius, 2025

TABLE OF CONTENT

LIST OF FIGURE

LIST OF TABLE

Notations

A_f – the cross-sectional area of SFRC bar;
A_s – the cross-sectional area of the reinforcement;
A_{s1} – the cross-sectional areas of the reinforcement in the tension zone;
A_{s2} – the cross-sectional areas of the reinforcement in the compression zone;
b – the width of the section;
B – the bending stiffness of the beam;
B_s – the short-term stiffness of reinforced concrete flexural members;
B_f – the short-term stiffness of SFRC reinforced concrete flexural members;
E_c – the elastic modulus of the concrete;
E_s – the modulus of elasticity of the reinforcement;
E_{s1} – the modulus of elasticity of the tensile reinforcement;
E_{s2} – the modulus of elasticity of the compressive reinforcement;
E_f – the modulus of elasticity of the SFRCbar;
f_r – the rupture modulus of concrete;
f_{tk} – the standard value of the tensile strength of concrete;
f_{cu} – the compressive strength generally measured with a standard specimen of concrete in a cube of 150mm*150mm*150mm;
f'_c – the compressive strength measured with a cylindrical concrete specimen of Φ150*600;
f_1 – the deflection calculated at bending moment M_1;
f_2 – the deflection calculated at bending moment M_2;
f_{cal} – the deflection calculated by new model and code technique (reinforced concrete beams);
f_{exp} – the deflection of the experimental beam (reinforced concrete beams);
$\overline{f}$ – the normalized deflection of reinforced concrete beams;
$\overline{f}_{FRP}$ – the normalized deflection of SFRC reinforced concrete beams;
f_{fcal} – the deflection calculated by new model and code technique
f_{fexp} – the deflection of the experimental beam ;
h_0 – the effective height of section;
h – the height of section;
I_{cr} – the converted moment of inertia of the cracked section;
I_g – the gross moment of inertia of concrete sections (ignoring reinforcement);
I_{ucr} – the converted moment of inertia of the uncracked section;
I_e – the effective moment of inertia of the section;
I_1 – moment of inertia of uncracked section (ignoring reinforcement), $I_1=I_g$;
I_2 – moment of inertia of a fully cracked section, $I_2=I_{cr}$;
I_t – the moment of inertia of a non-cracked section transformed to concrete;
K_r – deformation reduction factor;
L_0 – the calculated length;
m – mean;
M – the bending moment under consideration;
M_{cr} – the cracking moment;
M_u – the ultimate bending moment determined by the compressive strength of the concrete;

M_1 – the cracking moment, $M_1 = M_{cr}$;
M_2 – Three times the cracking moment, $M_2 = 3M_{cr}$;
M_y – the yield moment of the experimental beam assuming a yield strength of 500 Mpa for the reinforcement;
$\overline{\boldsymbol{M}}$ – load levels (reinforced concrete beams);
$\overline{\boldsymbol{M}}_{\boldsymbol{f}}$ – load levels (FRP reinforced concrete beams);
M_{fy} – the yield moment of the FRP bar experimental beam;
N_{ts} – the tensile stiffening force;
N_{s1} – the internal forces of tensile reinforcement;
N_{s2} – the internal forces of compressive reinforcement;
N_c – the internal force of compressive concrete;
y_t – the distance from the centroid of the section to the extreme tension fiber;
α_E – the ratio of the modulus of elasticity of the reinforcement to the modulus of elasticity of the concrete, $\alpha_E=E_s/E_c$;
α_b – the bond-dependent coefficient, for all FRP bar types, α_b =0.5;
α_{fE} - the ratio of the modulus of elasticity of the FRP bars to the modulus of elasticity of the concrete, $\alpha_E=E_f/E_c$;
β_1 – the coefficient for considering the bonding properties of reinforcement(when the steel bar is ribbed, β_1=1.0,When the steel bar is smooth, β_1=0.5);
β_2 – the coefficient for considering the type of load(when the load is a short-term load, β_1=1.0,when the load is a long-term, cyclic load, β_2=1.0);
β_d – the reduction coefficient used in calculating deflection;
γ – the factor that dependent on load and boundary conditions;
γ'_f - the ratio of the cross-sectional area of the tension flange to the effective cross-sectional area of the web, $\gamma'_f=(b_f\text{-b})h_f/(bh_0)$;
δ_{sq} – the stress in the longitudinal tensile reinforcement at the cracked section of the concrete member calculated as a combination of the short-term effects of the load;
δ_{fq} - the stress in the longitudinal tensile FRP bars at the cracked section of the concrete member calculated as a combination of the short-term effects of the load;
δ_1 – the deflections of uncracked sections;
δ_2 – the deflections of fully cracked sections;
$\overline{\boldsymbol{\varepsilon}_{\boldsymbol{c}}}$ – the average strain of concrete in compression zone;
$\overline{\boldsymbol{\varepsilon}_{\boldsymbol{s}}}$ – the mean strain of tensile reinforcement;
ε_c – the strains of the compressive concrete;
ε_{s1} – the strains of the tensile reinforcement;
ε_{s2} – the strains of the compressive reinforcement;
ζ - the distribution coefficient (when the member is in an uncracked state, $\zeta=0$);
η – the internal force arm factor of the reinforcement;
κ_i – the instantaneous curvature of the section;
κ – the curvature;
κ_{i1} – the instantaneous curvature when the section is not cracked;
κ_{i2} – the instantaneous curvature when the section is fully cracked;
κ_1 – curvature calculated at bending moment M_1;
κ_2 – curvature calculated at bending moment M_2;
μ – the expectation;
ξ – the comprehensive coefficient of average strain of concrete at the edge of compression;
ρ – the reinforcement ratio of longitudinal tensile steel bars;
ρ_{te} – the reinforcement ratio of longitudinal tension steel bars calculated according to the effective

tension concrete cross-sectional area, $\rho_{te}=A_s/(0.5bh_0)$;
ρ_f – the reinforcement ratio of longitudinal tensile SFRC bars;
ρ_{fe} – the reinforcement ratio of longitudinal tension SFRC bars calculated according to the effective tension concrete cross-sectional area, $\rho_{fe}=A_f/(0.5bh_0)$;
σ – the variance;
ψ - the uneven strain coefficients for longitudinal tensile reinforcement between cracks;
ψ_f - the uneven strain coefficients for longitudinal tensile SFRC bars between cracks;

Abbreviations

RC – Reinforced concrete;
SFRC – Steel Fiber reinforced concrete;
CV – Coefficient of variation;
SD – Standard deviation;
ACI – American concrete institute;

INTDODUCTION

Reinforced concrete structures, having been employed for nearly 180 years, find extensive applications across various engineering domains, including hydraulics, construction, transportation, and ports. Their widespread use is attributed to numerous advantages such as economic cost, overall structural performance, and the availability of materials. In comparison to structures constructed from alternative materials, reinforced concrete structures dominate various engineering projects. However, during the operational lifespan of these structures, exposure to different loads can lead to deformations. Excessive deformations can pose serious risks to the structure, including:

1. **Significant Reduction in Internal Forces:** Excessive deformations may result in a substantial decrease in the internal forces or load-carrying capacity of the structure.
2. **Impact on Important Building Functions:** Deformations can impact the functionality of critical buildings, affecting their intended use.
3. **Damage to Connected Elements:** Deformations may cause damage to interconnected building elements, compromising the overall structural integrity.
4. **Psychological Insecurity:** Exterior damage to a building can instill psychological insecurity among its occupants.

In the service period of concrete structures, accurate deflection control is crucial, as it directly influences serviceability and safety. Civil engineering designers must address deflection control during the structural design phase. The conventional method for deflection control involves calculating deflections under specified conditions and comparing them with limits outlined in building regulations. Consequently, extensive experimental research and theoretical discussions on deflection prediction for reinforced concrete members have been conducted globally.

Branson (1965) proposed a method for calculating deflection based on the effective moment of inertia, adopted by many countries' design codes. However, subsequent studies have revealed that the Branson model tends to underestimate deflections in flexural members with less reinforcement ratios. To address this, the assumptions of the Branson model are partially revised in this study. A new effective moment of inertia model is proposed based on these revisions to enhance the accuracy of deflection predictions.

As reinforced concrete structures become more prevalent, the issue of structural damage arising from the corrosion of reinforcing steel is gaining prominence. Fiber Reinforced concrete (SFRC) bars, with their excellent corrosion resistance, have emerged as a key focus in corrosion-resistant structural research. The use of SFRC bars in reinforced concrete structures is on the rise. Hence, investigating the accuracy of theoretical models for the deflection of SFRC-reinforced concrete structures holds significant theoretical and practical importance in addressing the challenges posed by corrosion

Relevance of the thesis

Flexural members are the most widely used elements in civil engineering, and reinforced concrete beams are the most representative elements of flexural members. The calculation of the deflection of flexural members is a very important part of structural design. Therefore, for the deflection calculation of flexural members, the design codes of various countries are based on the test, and the calculation formula is obtained by analyzing the test data and test phenomena. They all provide convenient methods for civil engineers. However, the research and code revision of concrete structures will be affected by subjective and objective conditions, experimental conditions, the number of components and other factors, and the existing codes will have defects and imperfections.

Most of the current design approaches for steel fiber reinforced concrete (SFRC) elements require the knowledge of the residual strength of (SFRC) in tension with the latter characteristic being obtained from standard bending tests. The involvement of extra tests hampers a wider application of such structures in practice. Recently by Kaklauskas and Sokolov proposed a curvature model for SFRC bending members that does not require the characteristic of the residual strength. The current study aims at investigating accuracy of curvature predictions by the design code methods and the new model.

Research object

The object of the study is the short-term deflection of concrete beams reinforced with steel and fiber bars. The main focus of the thesis is on the results of the new curvature model for predicting the deflection of concrete beams reinforced with steel bars and fibers.

Aim of the thesis

The thesis aims to examine the accuracy of the new curvature model in predicting the deflection of RC and SFRC beams.

Tasks of the thesis

In order to achieve the objectives of the article, the following problems need to be addressed：

1) To review the methods for deflection analysis of concrete beams reinforced with steel bars and fibers.

2) Collect experimental data from the literature on deflections of concrete beams reinforced with steel bars and fibers bars.

3) To examine the accuracy of the new curvature model for predicting deflection of reinforced concrete beams reinforced with steel bars and fibers bars.

4) To suggest some directions for future investigations.

Research methodology

The methodology adopted for the present research covers the collection and statistical analysis of experimental curvature/deflection results of RC and SFRC beams available in published literature and comparison of available deflection models.

Structure of the master’s thesis

The first chapter of the thesis is a literature review. This chapter reviews the methods of calculating deflection of reinforced concrete beams and the design codes between the various countries. Because the calculation of some material properties is specified differently under different design codes, this can have a significant impact on deflection calculations, so this part is considered in the literature review.

Second chapter focuses on the different material properties of fibers reinforcement compared to steel reinforcement.

Research novelty

In this study, the accuracy of the new curvature model proposed by Kaklauskas and Sokolov for predicting the deflection of reinforced beams reinforced with steel and fiber bars is verified using experimental data collected from the literature on reinforced beams reinforced with steel or fiber bars. Combined with the comparison with design code techniques, the superiority of the new curvature model for deflection prediction is demonstrated.

1 ADVANCED CHARACTERIZATION AND MODELLING OF (SFRC) AND REVIEW OF DEFLECTION STUDIES

This chapter provides a comprehensive overview of the literature and establishes a foundational context for the analysis of steel fibre reinforced concrete (SFRC). It begins with a concise historical account of the evolution of research, practical applications, design approaches, and standardization efforts related to fibre reinforced concrete (FRC). This historical context highlights the progress and developments that have led to the current understanding and utilization of FRC in construction and structural applications.

The chapter then delves into the classification of FRC, outlining the main categories and distinguishing features that differentiate various types of fibre-reinforced materials. It further examines the modeling approaches employed to describe the constitutive behavior of tensile SFRC, providing insights into the theoretical frameworks and methodologies used to capture its mechanical properties. Particular attention is given to how these models address the tensile performance, which is a critical aspect of SFRC's structural behavior.

A detailed discussion follows on the key material characteristics, underlying mechanisms, and influential factors that shape the properties of SFRC. These include the role of fibre type, distribution, orientation, and bonding with the matrix, as well as the interaction of these factors under different loading conditions. The chapter also highlights the interplay between material properties and performance, emphasizing how these parameters contribute to the enhanced durability, toughness, and post-cracking behavior of SFRC.

The review of test methods and design techniques is an integral part of this chapter. It examines various experimental approaches used to assess the mechanical properties and post-cracking performance of SFRC. Among these, the standard prism bending test is discussed in detail due to its widespread use and significance in characterizing the material's flexural behavior.

Additionally, the chapter explores design guidelines and recommendations that inform the practical use of SFRC in construction, focusing on techniques for optimizing its performance and ensuring compliance with engineering standards.

The chapter also addresses the serviceability behavior of SFRC elements reinforced with steel bars, providing an analysis of how the integration of steel reinforcement impacts the overall performance and durability of SFRC structures. The discussion includes modeling strategies for

serviceability, shedding light on the interaction between steel bars and fibre reinforcement in various structural scenarios

1.1 Applications of Fibre Reinforced Concrete in Structural Engineering

1.1.1 Evolution and Practical Uses

the past few decades, fiber-reinforced concrete (FRC) has become a versatile and widely adopted construction material, offering significant improvements over plain concrete and traditional reinforcement methods. Extensive research and practical applications have demonstrated its potential, establishing FRC as a globally recognized material in various construction sectors. While plain concrete excels in compressive strength, its brittleness under tension is a significant drawback. When tensile stresses exceed its capacity, cracks form and propagate rapidly, often leading to failure. Historically, fibers have been used to address this limitation, dating back to ancient times when materials like straw and horsehair were added to mud bricks in Babylonian and Egyptian construction. In modern usage, fibers enhance tensile strength and delay the spread of micro-cracks, allowing the material to sustain greater loads after cracking.
Research has shown that fiber reinforcement significantly improves post-cracking energy absorption (toughness) while having minimal impact on the initial cracking strength of the concrete matrix. Today, fiber reinforcement is recognized as an efficient alternative to traditional steel bars, improving labor conditions and productivity in construction and prefabrication. In certain structural elements such as foundations, walls, or slabs on grade, fibers can replace conventional reinforcement entirely. In beams and slabs, fibers often complement traditional or pre-stressed reinforcement, providing economic benefits and improving construction efficiency. Structurally, fibers enhance fracture resistance and overall performance by bridging cracks as they form, improving both serviceability and ultimate load capacity. Under service loads, fibers contribute to increased flexural stiffness, reduced crack widths, and better crack spacing. In ultimate load conditions, fibers enhance load capacity and ductility, particularly in shear and punching resistance. However, their impact on pre-cracking behavior is relatively minor.

1.1.2 Advances and Challenges in Fiber-Reinforced Concrete

In recent years, significant progress has been made in understanding the material properties and structural behavior of steel fiber-reinforced concrete (SFRC). These advancements have led to

improved analysis of FRC elements. Despite this progress, SFRC remains predominantly used in non-critical load-bearing applications.

A major limitation to broader adoption is the lack of universally accepted design standards. While several guidelines have been introduced, their differing approaches have hindered consistent implementation. For SFRC to realize its full potential in load-bearing structures, harmonized design standards are essential. These should include comprehensive recommendations for selecting fiber and concrete properties, implementation strategies, and standardized testing methods. Such advancements would enable engineers to leverage the unique benefits of SFRC more effectively in structural design.

1.1.3 Advancements in Fiber-Reinforced Concrete Technology

The development of fiber-reinforced concrete (FRC) has led to an array of cement-based materials incorporating various fibers, showcasing notable improvements in both mechanical and structural properties. This progress, particularly since the inception of concrete technology, includes advancements in strength, workability, ductility, and permeability (Li & Fischer 2002; Dupont 2003). The properties of FRC are largely dictated by the type and characteristics of the fibers used, which range from traditional steel to synthetic materials like glass, carbon, polypropylene (PP), and polyvinyl alcohol (PVA).

1.2 Fiber Characteristics and Types

1.2.1 Fibre reinforced concrete (FRC).

Plain concrete is a brittle substance material with high compressive strength in compare to tensile one which is around ten times smaller. Thus, the implementation of reinforcement is essential to improve the tensile properties of the material. The standard method involves the placement of the steel reinforcing bars to increase to boost the load carrying capacity in the zones subjected to considerable tensile and shear stresses.

Relatively new approach lies in the enhancement of concrete tensile strength by means of material modification which includes the addition of fibers to the concrete mix (Sutera, 2019).

The main purpose of the fibers is to bear the tensile stresses once the concrete element is cracked. Besidesthe tensile strength improvement, fibers could influence on other properties of concrete such ascrack resistance, durability, fire resistance, fatigue resistance, ductility, etc. Also, it should be mentioned that the fiber could be added to the concrete mix for structural and non-structural purposes (Sutera, 2019).

Generally, we can classify as structural fibers, those which considerably increase the breaking energy of the concrete in comparison with the plain one (in this case, their contributionshould be considered in the design of the FRC elements) (Sutera, 2019). Non-structural fibers, in turn, are notto be considered in the design procedure as they are aimed to effect on certain properties which were described above (Sutera, 2019).

1.2.2 Fibres type

A variey of parameters influence the properties and behavior of fiber reinforced concrete, including mechanical properties of the fibers used and their geometrical shape, for instance. Each fibre type is developed for a specific purpose which couldbe the improvement of tensile strength, controlling drying shrinkage or the improvement of fireresistance.

One of the most essential parameter for the fibre is its geometrical characteristics which vary crucially depending on the specific purpose: fibers could be several millimeters of length (microfibers) up to 80 mm (macro-fibers). The diameters also differ significantly, from

fraction of a micrometer to 2 mm. Also, the shape of the fibre should be taken into considerationdue to impressive diversity of this aspect: they can be straight, wave-shaped, bow-shaped, toothed, the surface intended, twisted or irregular, as illustrated in Figure 1. The cross-section of fibres can be different and can have a circular, square, rectangular, triangular, elliptical and irregular cross-section as it is presented in Figure 2. Besides, in order to improve the adherencewith the concrete, the fibers can present the shaped ends, undulations, corrugations, crushing, hooks, etc. (Sutera, 2019)

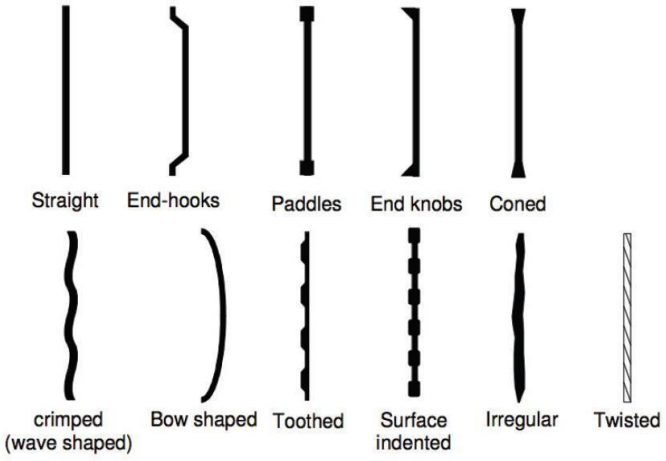

Figure 1:Type of steel

The mechanical properties of the fibres and their variety in dependence on the material couldbe noted in the Table 1.

Table 1: Physical properties of typical fiber

Fibre	Density (g/cm³)	Tensile Strength (MPa)	Young's Modulus (GPA)	Elongation at Break (%)	Length (mm)	Diameter (µm)
Synthetic						
E-glass	2.5–2.59	2000–3500	70	2.5	-	-
Aramid	1.4	3000–3150	63.0–67.0	3.3–3.7	-	-
Carbon	1.4	4000	230.0–240.0	1.4–1.8	-	-
Natural						
Bamboo	0.6–1.1	140–800	11–32	2.5–3.7	1.5–5.4	25–400
Kenaf	1.2	223–930	11–60	1.6	-	-
Flax	1.4–1.5	345–2000	27.6–103	2.7	5–900	10–100
Sisal	1.33–1.5	363–700	9.4–22	2.0–2.5	2–5	50–200
Hemp	1.48	550–900	23.5–90	1.6	5–55	25–50
Coir	1.15–1.46	95–230	4–6	15–40	20–150	10–460
Ramie	1.0–1.55	400–1000	24.5–128	2.0–3.8	900–1200	20–80
Abaca	1.5	400–980	6.2–20	1.0–12	-	-
Baggase	1.25	222–290	17.2–27.1	1.1–10	10–300	10–34
Cotton	1.5–1.6	287–800	5.5–12.6	3.0–10.0	10–60	10–45

From the presented in Table 1 types of fibers, steel fiber are the most commonly employed in structural applications among the type of fibrates instead in Table 1.given that this thesis focuses on elevated slabs which are subject to significant stresses the above mentioned type of fibers will be discussed in greater detail.

1.2.3 Steel fibres

The steel fibers for concrete mix are discontinuous, with a discrete and uniform distribution that resulting a high degree of homogeneity and isotropy. steel fibres typically rang in diameter 0.25 mm and 0.80 mm in diameter and the length is in the rangefrom 10 to 75 mm.
The following parameters are used to characterize steel fibers:

Slenderness often known as aspect ratio: it is the connection between the length of the fibre and its diameter $(\frac{l_f}{\phi_f})$.

The tensile strength: this parameter depends on the quality of the steel. For a low or medium carbon content, the average resistance oscillates between 400 and 1500MPa, while it could reach 2000Mpa with higher carbon content.
Shape: It has great importance for the adherence between fibre and concrete, as shownin chapter 2.1.1. It could be appreciated the variety of possible shapes in more detail bymeans of .

Figure 2: types of steel fibres (Sutera, 2019)

It is advised the fiber length be at least twice as long as the larger aggregate. still fiber are Therefore typically 2.5 to 3 times longer than the maximum aggregate size.Furthermore, the length of the fiber must be less than two thirds of the pumping pipes diameter or less. However, the length of the fiber must be sufficient to give the necessary adhesion to the matrix and to avoid pull-outs too quickly.

1.2.4 Steel fibre reinforced concrete

Steel fibre reinforced concrete (SFRC) is widely used extensively in serval construction related fields. The properties of steel fibers allow to improve both structural and non-structural characteristics of the material. However, it should be mentioned that because of the enhanced mechanical and geometrical properties of the fibers and the appearance on new codes and guidelines as it was stated previously. Nowadays, the presence of fibers in the concrete mix is able to provide the partial or even total substitution of the conventional reinforcement due to high residual tensile strength, ductility and toughness of the material in question.

Experimental studies have shown that that normally used fibre volume in concrete does notlead to an increased strength before cracking. (Sutera, 2019) The major role of the steel fibre reinforcement is to control the cracking of the concrete and give a contribution to the capacity after cracking.

The use of steel fibres is a well-acknowledged methodology to improve the tensile performance and toughness of concrete. Beside the better structural performances resulting from the enhanced mechanical properties, FRC allows a better shrinkage and crack control leading to increased structure durability. Stress redistribution resulting from the high internal redundancy of these structures may allow exploiting the post-cracking strength and toughness of SFRC, leading to a possible reduction of conventional reinforcement. The aforementioned partial or total substitution of conventional rebars allows reducing the construction time and costs in comparison with traditional Reinforced Concrete (RC) structures. (Sutera, 2019)

1.3 Material Properties of Steel Fibre Reinforced Concrete

1.3.1 Compression

Numerous researchers (Ezeldin & Balaguru 1992, Hsu & Hsu 1994, Someh & Saeki 1994, Mansur *et al.* 1999, Nataraja *et al.* 1999, Bencardino *et al.* 2008, Riz- zuti & Bencardino 2014) have investigated the effect of steel fibres on the com- pressive behaviour of SFRC. In most of the researches it was stated, that moderate volumes of fibres do not influence the compressive strength significantly. How- ever, addition of fibres causes a less brittle failure of compressive concrete (Meškėnas A. , 2018).

The stress-strain behaviour of plain concrete shows a linear-elastic response up to around 30% of the compressive strength and continuing with non-linear gradual increase up to the compressive strength. It is further followed by strain softening behaviour until concrete failure takes place by crushing. The compres- sive concrete failure is mostly related to the failure in tension, as tensile stresses are acting in perpendicular direction to the compressive load. The cracking pro- cess starts as sharing of the aggregate-cement paste interface and further propa- gates into the concrete matrix. The cracking process develops with an increasing compressive load while cracks become parallel to the direction of the principal compressive stress (Meškėnas A. , 2018).

Although the ascending branch of the compressive stress-strain relationship is only slightly altered by the addition of the fibres, fibre reinforced concrete demonstrates less abrupt descending

branch of the stress-strain curve than plain concrete. This results in a significant increase in the ductility and toughness of the fibre reinforced concrete. The main advantage of fibres is their capacity to resist the growth of the longitudinal cracks. However, the effect of fibres de- pends on the type, geometrical and mechanical properties of the fibres and the properties of the matrix. Generally, it can be observed that steel fibres at reasonable dosages (less than 1% by volume) have no influence to the pre-peak properties, whereas the strain at crack localization and the failure strain increase. However application of microfibers or with the fibre dosages greater than 1% the compress- sive behavior can be improved (Meškėnas A. , 2018).

1.3.2 Tension

When subjected to tensile stresses, prior to cracking, the behavior of plain con- crete is approximately linear. Close to the peak stress, the overall response be- comes softer due to micro-cracking and, as the tensile strength is reached with increased applied strain, a crack forms. Plain concrete, being a quasi-brittle mate- rail, can transmit tensile stresses, although at a low value, after cracking and is mainly attributed to aggregate interlocking (Meškėnas A. , 2018)The specimens overall tensile resistance diminishes quickly to zero after the onset of cracking.
The tensile strength and modulus of elasticity of FRC are not significantly affected by the addition of fibers. However, the fibers have a considerable impact on the tensile fracture behaviour and the fracture energy. The random orientation of fibres greatly enhances the post-cracking resistance, thereby ensuring a more ductile failure. The most characteristic material behaviour for FRC is shown after reaching the limit of elastic behaviour. This boundary is commonly referred to as the limit of proportionality (LOP) and represents the initiation of the post-cracking residual strength of FRC. The shape of the post-cracking curves vary significantly, mainly depending on the type, orientation and number of fibres crossing the crack plane and the properties of the concrete (Meškėnas A. , 2018)
It is generally accepted that the most appropriate and direct classification of the tensile behaviour is based on the uni-axial response (Hillerborg 1980, van Mier 1997, van Vliet & van Mier 1999, van Mier & van Vliet 2002, Löfgren 2005, Foster 2014) (Meškėnas A. , 2018). The tensile behaviour of cementitious materials can either be clas- sified as strain-softening or strain-hardening .
For strain softening materials, failure occurs over a localized single dominant crack. The behavior is characterized by the residual tensile strength of the specimen never reaching the tensile strength of the matrix after the limit of proportionality LOP (cracking), but tends to zero as the crack

widens. Strain-hardening occurs when the post-cracking strength properties are higher than the elastic ones after the limit of proportionality LOP is reached. The residual stress increases after first cracking, and this may result in multiple cracking within the sample, which is then followed by failure at a localized crack. Based on this classification, tensile properties for strain-softening steel fiber reinforced concrete will be discussed in the thesis.

There are several methods that are proposed in the literature to study the tensile behavior of FRC (Meškėnas A. , 2018)These include uniaxial tension test where the fracture toughness is used to characterize the post-peak behavior of the material or the FRC is tested in bending to determine the flexural toughness properties.

1.3.3 Mechanical properties

Steel fibres significantly increase the ductility of the concrete and also improve the residualtensile strength of the material. The main task of the added fibre is to bridge cracks that occur in the matrix and transfer tensile stresses across the cracks. The fibre contributes to improved crack control by causing large single cracks to be replaced by a system of microcracks with considerably smaller crack widths.

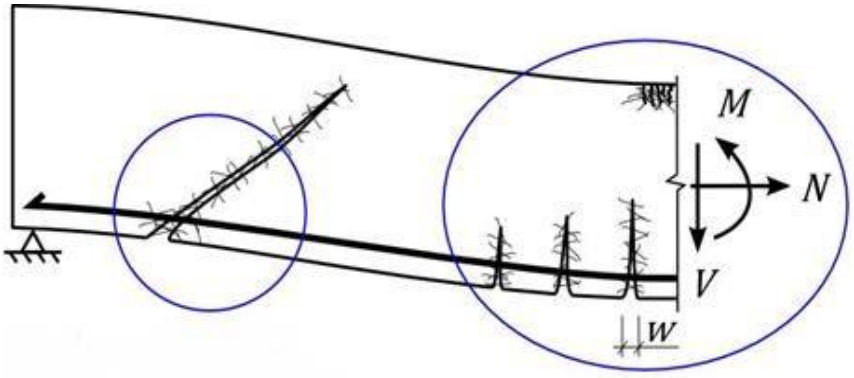

Figure 3: Effects of fibre on the structural behaviour (Sutera, 2019)

Several studies and tests carried out over the years has highlighted some important properties, The effect of fiber in terms of crack bridging under the application of sectional forcesM, V and N, Figure 4, are listed below. (Bischo., 2007) (Sutera, 2019)

- Increased shear resistance
- Increased punching resistance
- Increased dowel effect
- Inhibits growth of splitting cracks
- Increased confinement of anchored bars
- Reduced crack spacing
- Reduced crack widths
- Increased moment resistance
- Increased flexural stiffness
- Increased ductility in compression

The post-cracking behavior of concrete, however, is significantly improved due to the fiber contribution. SFRC obtains a significant increase in the ultimate tensile strain and displays a distinct and stable residual tensile strength after cracking, even as the crack widths increase. (Bischo., 2007) Factors that influence on the material properties of fiber-reinforced concrete are the individual material properties of the matrix and the fibers, respectively, and the bond strength between the matrix and fibers. Furthermore, the amount of fibres, the orientation and distribution of fibres within the matrix are of importance.

The fibers are generally mixed into the concrete before pumping the concrete into the formwork, and the aim is to obtain a random fibers distribution and orientation. The distributionand the orientation of the fibers may be prevented from distributing freely and can be influencedby factors such as the method of placement, equipment used, such as reinforcement bars, and properties of the fresh concrete.

The fiber contribution leads to a more ductile failure for SFRC than for plain concrete, and the failure is mainly caused by fiber pull-out. (Bischo., 2007) The tensile deformation capacity is improved,resulting in an increased critical crack opening. The critical crack opening is defined as the onewhere no stress can be transferred, as it is illustrated in Figure 4.

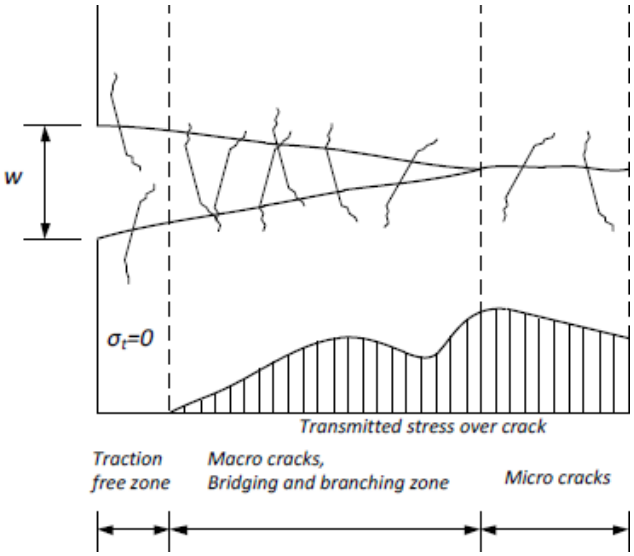

+ Figure 4: Steel fibre reinforced concrete cracking zones (Bischo., 2007)

While Figure 6, shows a real fracture surface of SFRC after failure due to fiber pull-out, inwhich the randomly distributed and oriented fibers are clearly displayed.

Figure 5: Fracture surface of steel fibre-reinforced concrete (Bischo., 2007)

Failure of SFRC due to fiber pull-out is desirable in order to obtain ductility and toughnessduring failure. Therefore, the fiber must be adequately ductile to prevent fiber fracture due to bending. Furthermore, the bond strength between the fiber and the matrix must be of the samemagnitude, or higher, than the tensile strength of the matrix. (Bischo., 2007)

For steel fibers with hooked ends a significant energy dissipation arises as the fiber is straightened and plastically deformed. This dissipated energy becomes part of the fracture energy of the concrete. The fracture energy is defined as the area under the stress-crack openingcurve in tension and is the energy required for crack propagation (Bischo., 2007) (Sutera, 2019) . Consequently, SFRC displays significantly higher fracture energy than plain concrete.

1.3.4 Residual flexural tensile strength

One of the most critical points in SFRC theory is to predict the tensile behavior of the material and especially to quantify the residual stresses in tension for a cracked section. After cracking, the SFRC displays a relatively stable residual tensile strength, even as the crack widths increase. The residual tensile strength, $f_{R,i}$, is defined as the residual tensile force resultant acting on a unit area of a cracked section in the concrete. During the design procedure, the contribution of fibres can be introduced by considering FRC as a homogeneous material with higher toughness, represented by the residual tensile strength.

Depending on the fibre content, the concrete might have strain-softening or hardening behaviour. A strain-softening material behavior is referred to as a behavior where the stress reduces with continuous development of plastic strains, whereas for strain-hardening material, the stress value increase after the crack deformation.

For deeper understanding of FRC behaviour, the uniaxial tension response of the material in question is showed in Figure 7. For strain-softening materials a localized single crack characterizes the tensile behavior, as seen in the tensile diagram.

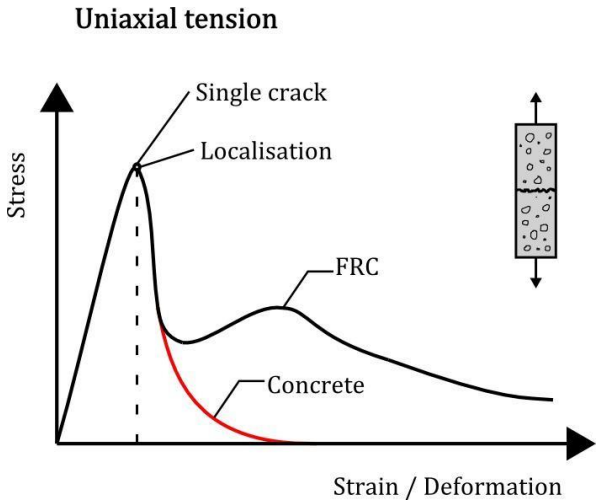

Figure 7: Tensile behavior of FRC in uniaxial stress state (Löfgren, 2005)

In comparison to plain concrete, neither the tensile strength nor the modulus of elasticity of fibre-reinforced concrete is significantly affected. The fibre mainly affects the tensile fracture behavior and the post-cracking properties. For FRC with a low to moderate fibre content (< 1%) the stress-strain curve is characterized by a strain-softening behavior, as shown in figure 7. After the tensile strength is reached, the curve in this case decreases relatively steeply, but whereas the curve for plain concrete continues decreasing until zero. The curve for FRC typically increases again as the fibre starts acting by carrying tensile stresses across cracks. The last part of the curve, having an approximately constant stress value, displays the residualtensile strength of the FRC.

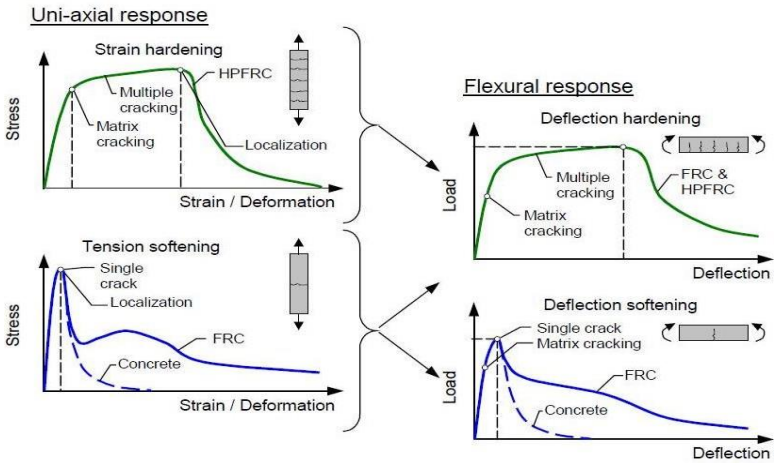

Figure 8: Typical tensile and flexural behavior of FRC (Löfgren, 2005)[i]

Figure 8 shows typical tensile and flexural behavior of FRC. As it could be appreciated in the figure above that FRC can provide deflection hardening in bending despite the softening response in uni-axial tension. Also, it could be noted that in the case of softening behavior, the deformations localize in one crack, while the hardening one leads multiple cracking before reaching the peak value. (Löfgren, 2005)

1.3.5 Measuring the flexural tensile strength

According to FIB model code (Sons, 2013), the strength of fibres is measured as a residual flexural tensile strength. This can be done by performing three point bending test (3PBT). The main principle of the test is to evaluate the behaviour of SFRC in terms of residual flexural tensile strength values determined from the load-crack mouth displacement curve or load-deflection curve obtained by applying a centre-point load on a simply supported notched prism. The FIB model code proposes that it is to be done in accordance with EN 14651 (2005). (EN, (2005). 14651: 2005+ A1: 2007)

The short description of the test procedure is: a simply supported beam with a span length of 500 mm and nominal size (width and depth) of 150 mm is to be tested. In the middle of the span, a notch is placed with a height of 25 mm and a maximum width of 5 mm, seen in Figure 9. A concentrated load is placed in the middle of the beam. The mentioned load should have the established rate of increase and at the same time the crack mouth opening displacement (CMOD) in the notch is to be measured. The result from the bending test of RILEM beam is shown in Figure 10 and 11

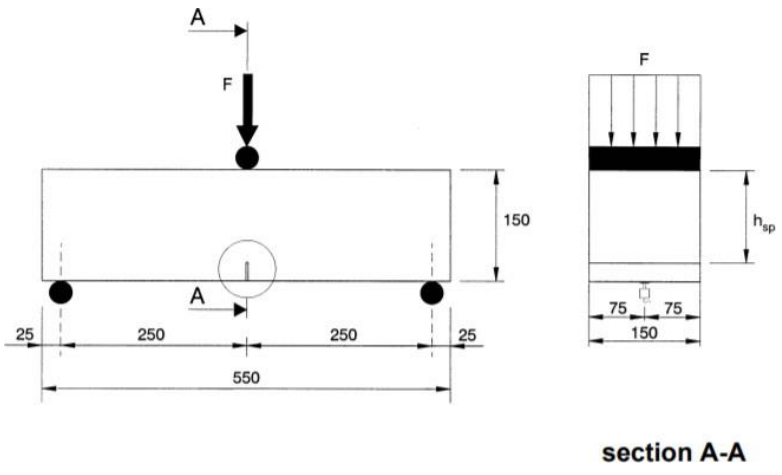

Figure 2:Typical arrangement for measuring CMOD (EN, (2005). 14651: 2005+ A1: 2007)

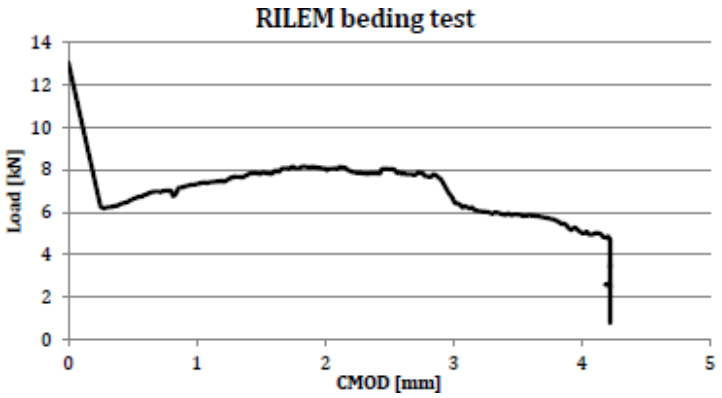

Figure 3:RILEM bending test (Löfgren, 2005)

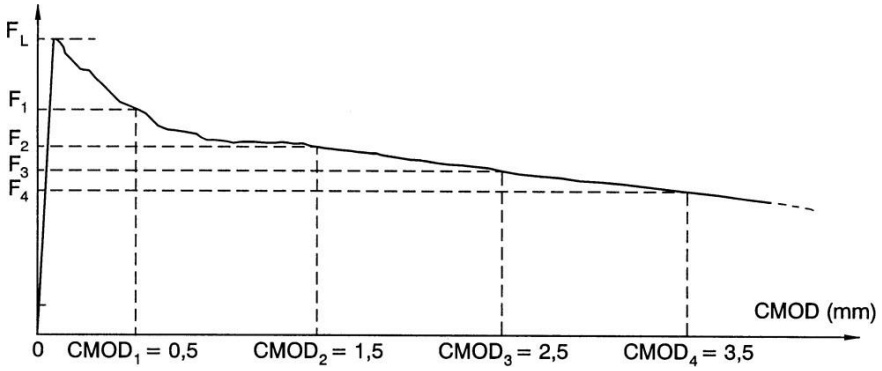

Figure 4: Crack Mouth Opening Displacement (EN, (2005). 14651: 2005+ A1: 2007)

Different values of the residual flexural tensile strength, $f_{R,i}$, should be evaluated according to the following equation

$$f_{R,j} = \frac{3F_j l}{sp} \tag{2.1}$$

Where

$f_{R,i}$ is the residual flexural tensile strength corresponding to $CMOD_i$, [MPa]

F_i is the load corresponding to $CMOD_i$, [kN]

$CMOD_i$ is the crack mouth opening displacement, [mm]

l is the span of the specimen, [mm]

b is the width of the specimen, [mm]

h_{sp} is the distance between the notch tip and the top of the specimen, [mm]

The values f_{R1} and f_{R3} are obtained from the corresponding $CMOD_1$ and $CMOD_3$, respectively(Figure 12)

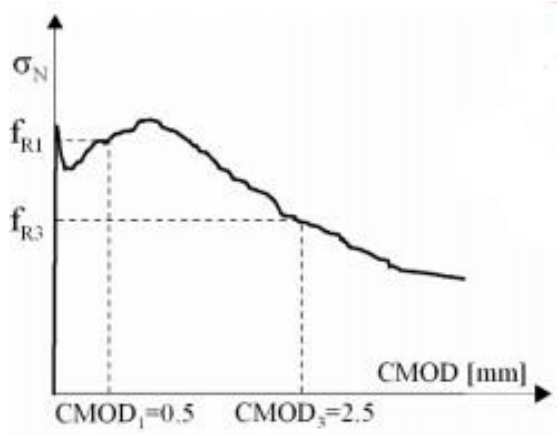

Figure 5: An example of typical results from a bending test with a softening material behaviour. (Sons, 2013)

By making certain adjustments to conventional concrete practice, it is possible to produce SFRC. The primary concern is to introduce sufficient amount of uniformly distributed fibers in concrete to achieve improvements in mechanical properties, keeping the concrete workable to permit proper mixing, placing, and finishing.

There are various procedures available for the mix design of SFRC. Typical recommended proportions are shown in Table 2. To provide better workability of concrete, amount of paste in the mixture should be increased. This requires a higher

cement content, or moving the ratio of fine aggregates to coarse aggregates upwards. Alternatively pozzolanic admixtures can be used to replace cement. The use of superplasticizers does not provide the ability to incorporate a higher steel fiber content; the cement paste becomes more fluid with the addition of superplasticizersand tends to run out of the fiber clusters as they are about to form. Segregation of fibers occurs approximately at about the same fiber content as for a mix with no superplasticizer addition. Regardless of the mix design, trial mixes should beprepared to ensure workability and strength properties .

Table 2: Range of Proportions for Normal Weight SFRC

Property	9.5 mm Maximum	19mm Maximum
	Aggregate Size	Aggregate Size
Cement (kg/m^3)	355-590	300-535
w/c ratio	0.35-0.45	0.40-0.50
Fine/coarse aggregate (%)	45-60	45-55
Entrained Air (%)	4-7	4-6
Fiber Content (%) by volume		
Smooth steel	0.9-1.8	0.8-1.6
Deformed steel	0.4-0.9	0.3-0.8

1.3.6 Mixing, Placing, and Finishing of SFRC

Mixing: Various methods are available for introducing steel fibers to concrete, either with the dry constituents, or to the wet mix. These methods range from charging the aggregate conveyor with fibers sieving directly into the mixer drum, or sieving the fibers and blowing them into the drum. Uniform distribution of fibers throughout the mix is very important. For steel fibers, no special mixing technique is required; however, adjustments in the mix proportion, mixing sequence, and rate of addition of constituents may be necessary.

mixer individually without clumping and be immediately removed from the point of entry by the mixing action. Besides fiber addition rate should be comparable with the mixing speed. Primary problem encountered in mixing of SFRC is formation of fiber balls. The most common causes of wet fiber balling are over mixing and using a mixture with too much aggregate content, typically more than 55% of the total combined aggregate by absolute volume. Most fiber balling occurs somewhere before the fibers are added to the mixture. This means that, if the fiber balls form, it is because fibers were added in such a way that they fell on each other and stacked up (Shah, 1993).

Placing: Generally, SFRC with a proper cement content and water-cement ratio seems to be relatively stiff and unworkable, compared to conventional plain concrete. Water-cement ratios for SFRC mixtures should be carefully controlled, as it is very easy to add unnecessary water to the mixture causing the loss of many benefits obtained by steel fiber inclusion without providing any improvement in workability. SFRC in the fresh state tends to hang together and resist movement during compaction. However, SFRC responds well to vibration. Internal vibration should be applied with care to avoid fiber free zones, which is formed by scattering of fibers leaving a zone unreinforced. Pumping SFRC is a common method of placement (Shah, 1993).

Finishing: SFRC can be finished by using conventional methods; however certain refinements in techniques and workmanship are required. For flat-formed surfaces, normally no special attention is needed. If chamfers or rounds have been provided at the edges and in corners, the ends of fibers will not protrude at these points when forms are removed. To provide added compaction and bury surface fibers, open slab surfaces should first be struck off with a vibrating screed. Magnesium floats can be used to establish a surface and close up any tears or open areas, which are caused by the screed. Throughout all finishing operations, care must be taken not to overwork the surface. Overworking may bring excessive fines to the surface (Shah, 1993).

1.3.7 Practical Applications of SFRC

The uses of SFRC are so varied, and making a categorization is difficult. Their rangeis shown in Figure 6. Applications include stairways, pavements, airport pavements,slabs, tunnel linings, shotcrete, refractory elements, and various types of concrete repair. The application areas of SFRC are expanding through the accumulation of research conducted on this topic, but unfortunately approximately 1% of steel fiber addition to concrete almost doubles the cost, so the use of SFRC is limited to specialapplications.

1.4 Constitutive Modelling of Steel Fibre Reinforced Concrete in Tension

1.4.1 Classification of the Test Methods

To accurately determine the material properties of Steel Fibre Reinforced Concrete (SFRC), various test methods are recommended in design guidelines. These methods can be classified based on two primary distinctions: direct versus indirect methods, and quantitative versus qualitative methods.

In direct methods, the material properties are derived directly from the test results. A notable example is the uniaxial tension test, where stress-strain or stress-crack opening relationships can be directly obtained from the test. This method provides the most accurate and straightforward way to characterize tensile properties, but it is often challenging to perform due to issues related to specimen preparation, alignment, and loading control.

Indirect methods of testing tensile behavior rely on interpreting and deriving material properties using established correlations. Examples include splitting tensile strength tests and flexural tests. While these tests do not directly measure tensile stress, they enable the calculation of tensile properties based on observed behaviors. For instance, flexural tests involve bending beams or other elements, with tensile strength derived using specific formulas to convert flexural data into tensile behavior.

Test methods can also be classified based on their purpose: quantitative or qualitative. Quantitative methods determine specific physical properties, such as tensile strength, fracture energy, or deformation characteristics. In contrast, qualitative methods are used for comparison, such as evaluating different SFRC mixes, fiber types, or compositions against a reference. For example, a qualitative test might compare various fibers by assessing energy dissipation, peak load capacity, or toughness relative to a baseline mix.

Various testing methods exist for evaluating the tensile behavior of SFRC, either directly or indirectly. Among these, the direct tension test is considered the most reliable for obtaining key material data, especially residual strength parameters. For uniaxial tensile strength determination, tests on un-notched specimens provide a clear representation of tensile strength before cracking. To capture the stress-crack width relationship post-cracking, notched specimens are used, allowing controlled crack initiation and propagation during testing. Despite its reliability, the direct tension test can be complex to perform and requires meticulous preparation to ensure proper alignment and minimize unintended stress concentrations.

In practical applications, bending tests on prismatic beam specimens are the most commonly employed method to characterize the post-cracking behavior of SFRC. These tests typically use three-point or four-point bending configurations. In three-point bending, a single central point applies the load, while four-point bending involves two load points, distributing stress more evenly for a controlled response. To ensure predictable crack localization, notches are often introduced in the specimens.

Bending tests derive uniaxial tensile strength and residual strength through formulas that convert flexural responses into equivalent tensile properties. Other methods, such as round determinate panel tests or splitting tensile tests, can also be used to characterize SFRC. However, while bending tests provide insights into post-cracking behavior, their results differ significantly from those of uniaxial tension tests.

In flexural bending tests, materials may exhibit deflection softening or deflection hardening. Deflection softening occurs when load-carrying capacity decreases with increasing deflection, while deflection hardening refers to an increase in capacity as deflection progresses. Interestingly, a material showing strain softening in uniaxial tension may display either deflection hardening or softening during a bending test, adding complexity to result interpretation.

The dimensions of test samples also influence flexural test outcomes. Research shows that the size or height of beams can significantly impact results, sometimes causing contradictory outcomes. For instance, the same material might exhibit deflection hardening in one configuration and deflection softening in another. Therefore, careful consideration of sample dimensions and testing methods is essential for accurately evaluating SFRC properties.

1.4.2 Criteria and Characteristics

The tensile behavior of Steel Fibre Reinforced Concrete (SFRC) is influenced by numerous parameters, making it challenging to model its material behavior accurately. Due to this complexity, no single constitutive law can universally describe SFRC's post-cracking response. Two widely used non-linear approaches are the stress-crack opening relationship (σ-w) and the stress-strain relationship (σ-ε). These approaches provide critical insights into SFRC's post-cracking behavior, essential for structural design and material characterization. To investigate SFRC's post-cracking behavior, direct and inverse techniques are employed. Direct methods predict behavior based on predefined material models, while inverse methods derive model parameters from experimental test results. The inverse approach is particularly useful for calibrating models with real-world data, improving the accuracy of simulations for practical applications.

The stress-crack width (σ-w) approach characterizes post-cracking tensile deformation by relating tensile stresses to the crack opening displacement. The fictitious crack model, initially developed for plain concrete, provides a framework for this approach. In plain concrete, after cracking, a cohesive zone transfers stresses across the crack plane until the aggregate interlock effect dissipates. In SFRC, however, steel fibers bridge the crack, allowing stress transfer even as the crack widens. These fibers provide residual tensile strength post-cracking by resisting pull-out or rupture, contributing to the material's toughness.

Another common method to describe SFRC's behavior is the stress-strain (σ-ε) relationship, which is particularly useful in tension and compression applications and is widely applied in finite element analysis. This approach provides a straightforward representation of SFRC's elastic and post-elastic behavior, making it valuable for structural design. The σ-ε relationship accounts for the deformation within the gauge length, including both elastic deformation and crack-induced displacement.

The concept of characteristic length plays a key role in interpreting the σ-ε relationship. Introduced to bridge smeared-crack and discrete-crack models, it enables accurate conversion of total deformation into relative strain. During the linear-elastic phase, strain is calculated by dividing deformation by the gauge length. Post-cracking, the deformation reflects both the elastic response of un-cracked material and the crack opening displacement. By incorporating characteristic length, engineers can translate between modeling approaches, ensuring accurate simulations of SFRC behavior.

However, determining characteristic length is complex and influenced by factors such as fiber type and volume, matrix strength, geometry, reinforcement, and load levels. These factors affect crack propagation and fiber-matrix interactions, requiring careful calibration of characteristic length for specific applications to ensure precise results.

In summary, SFRC's tensile behavior is best captured by the stress-crack opening relationship (σ-w) and the stress-strain relationship (σ-ε). Both methods highlight the intricate interplay between fibers, the concrete matrix, and cracking. Direct and inverse analyses enhance the understanding and prediction of SFRC's performance, providing engineers and researchers with indispensable tools for optimizing its use in structural applications. These approaches continue to advance SFRC's potential for load-bearing and impact-resistant structures, despite the inherent challenges in modeling its behavior.

Direct analysis provides a straightforward method for modeling SFRC structures. This approach involves specifying the form of the constitutive relationship to simulate the material's behavior accurately. The parameters that define this constitutive law can be sourced either directly from experimental data, as outlined in various standards and guidelines (RILEM TC 162-TDF 2002a, JCI-S-002 2003, JCI-S-003 2007, CNR-DT204 2007, DBV 2007, EN14651 2007, DAfStb-Richtlinie 2010, Model Code 2010), or from specific characteristics of the material itself (Li et al. 1993, Prudencio et al. 2006, Luccioni et al. 2012, Naaman 2003b). Nevertheless, the variability in test results and inherent material properties often leads to inaccuracies in this direct modeling approach.

Conversely, inverse analysis employs an iterative method that adjusts to fit experimental data, thereby determining the parameters that shape the constitutive diagram. While this technique can effectively approximate the structural behavior of SFRC elements, it comes with its own set of challenges. Primarily, the inverse approach necessitates experimental evaluations involving various combinations of fibers and concrete properties. Often, the properties of SFRC derived from laboratory experiments do not match those observed in real-world applications due to differences in the production processes such as casting, flow, and vibration, which influence the fiber distribution and orientation. The success of this experimental fitting largely depends on the chosen form of the constitutive diagram and the acceptable range of deviation (Dupont 2003, Sousa & Gettu 2006, Kaklauskas et al. 2011, Gribniak et al. 2012).

Both methodologies, while useful, highlight the complexities involved in accurately modeling the behavior of SFRC structures and underscore the necessity for careful consideration of the material properties, experimental setup, and modeling assumption

1.5 Constitutive Models

1.5.1 Constitutive models in European codes and recommendations

Identification of the models

The identification of the most suitable constitutive model to simulate the tensile post-cracking behavior represents one of the key steps in the design of FRC structures. Over the past ten years several technical guidelines have been published with the aim of facilitating the design of these structures (Soranakom, (2009). Table 1 presents the constitutive models proposed by European standards (Beton-Verein, 2001)
(Code, 1993) grouped according to the type of diagram (namely rectangular, bilinear and trilinear or multilinear). The same table also summarizes the main parameters that define each one of the models and includes the schematics of the tests required to obtain the values of these parameters

Diagram	Parameters	Characterization test	
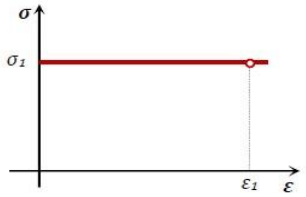	$\sigma_1 = f_{eq,ctd,II} = f_{eq,ctk,II} \cdot \alpha_f \cdot \alpha_{sys} / \gamma_{cf} \leq f_{eq,ctd,I}$ (α_{sys}: coefficient for size effect; α_f: coefficient for long-term strength behaviour) $\varepsilon_1 = \varepsilon_u = 10‰$	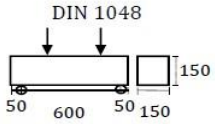	DBV
	$\sigma_1 = f_{Ftu} = f_{eq2}/3$ $\varepsilon_1 = \varepsilon_u = [20‰$ softening ; $10‰$ hardening]	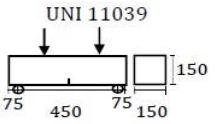	CNR-DT 204
	$\sigma_1 = f_{ctRd} = 0.33 f_{R,3,d}$ $\varepsilon_1 = \varepsilon_u = [20‰$ bending; $10‰$ tensile]	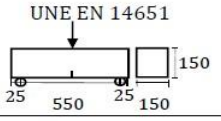	EHE-08
	$\sigma_1 = f_{Ftu} = f_{R3}/3$ $\varepsilon_1 = \varepsilon_u = [20‰$ softening ; $10‰$ hardening]	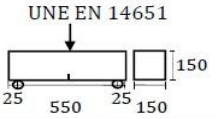	MC2010
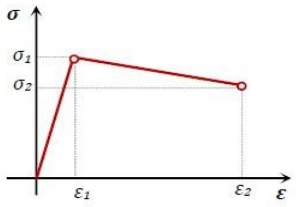	$\sigma_1 = f_{eq,ctd,I} = f_{eq,ctk,I} \cdot \alpha_f \cdot \alpha_{sys} / \gamma_{cf}$ $\sigma_2 = f_{eq,ctd,II} = f_{eq,ctk,II} \cdot \alpha_f \cdot \alpha_{sys} / \gamma_{cf} \leq f_{eq,ctd,I}$ $\varepsilon_2 = \varepsilon_u = 10‰$	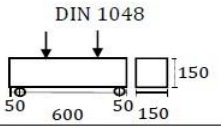	DBV
	$\sigma_1 = f_{Fts} = 0.45 f_{eq1}$ $\sigma_2 = f_{Ftu} = k[f_{Fts} - (w_u/w_{i2})(f_{Fts} - 0.5 f_{eq2} + 0.2 f_{eq1})]$ k=[0.7pure tension, 1 other cases] $\varepsilon_2 = \varepsilon_u = [20‰$ softening; $10‰$ hardening]	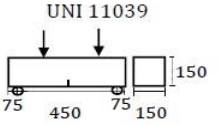	CNR-DT 204
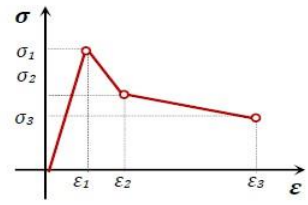	$\sigma_1 = f^f_{ctd} = \alpha_{fc} \cdot f_{ctk,fl} / \gamma^f_{ct}$ $\sigma_2 = f_{eq,ctd,I} = f_{eq,ctk,I} \cdot \alpha_f \cdot \alpha_{sys} / \gamma_{cf}$ $\sigma_3 = f_{eq,ctd,II} = f_{eq,ctk,II} \cdot \alpha_f \cdot \alpha_{sys} / \gamma_{cf} \leq f_{eq,ctd,I}$ $\varepsilon_1 = \sigma_1/E_c$; $\varepsilon_2 = \varepsilon_1 + 0.1‰$; $\varepsilon_3 = \varepsilon_u = 10‰$	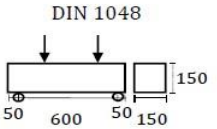	DBV
	$\sigma_1 = 0.7\, f_{ctm,fl}\,(1.6-d)$; $\sigma_2 = 0.45 \cdot \kappa_h \cdot f_{R,1}$; $\sigma_3 = 0.37 \cdot \kappa_h \cdot f_{R,4}$ $\varepsilon_1 = \sigma_1/E_c$; $\varepsilon_2 = \varepsilon_1 + 0.1‰$; $\varepsilon_3 = \varepsilon_u = 25‰$	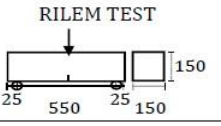	RILEM
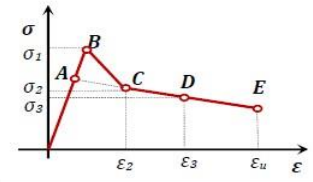	$\sigma_1 = f_{ct,d} = 0.6\, f_{ctfl,d}$ $\sigma_2 = f_{ctR1,d} = 0.45 f_{R,1,d}$ $\sigma_3 = f_{ctR3,d} = k_1(0.5 f_{R,3,d} - 0.2\, f_{R,1,d})$ $\varepsilon_2 = 0.1 + 1000 \cdot f_{ct,d} / E_c$ $\varepsilon_3 = 2.5/l_{cs}$ (l_{cs}: characteristic length) $\varepsilon_u = [20‰$ bending; $10‰$ pure tension]	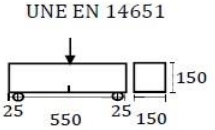	EHE-08
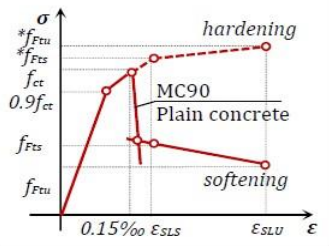	$f_{ctm} = 0.30 (f_{ck})^{2/3}$ $f_{Fts} = 0.45 f_{R1}$ $f_{Ftu} = k[f_{Fts} - (w_u/CMOD_3)(f_{Fts} - 0.5 f_{R3} + 0.2 f_{R1})]$ $\varepsilon_{SLS} = CMOD_1 / l_{cs}$ $\varepsilon_{SLU} = w_u/l_{cs} = \min(\varepsilon_{Fu}, 2.5/l_{cs} = 2.5/y)$ ε_{Fu} = [20‰ softening; 10‰ hardening]	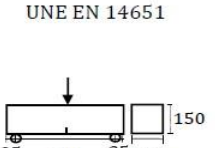	MC2010

Table 3:Constitutive models in European guide (Blanco Álvarez, 2013)

fib Model Code (2010)

The deeper knowledge gained on FRC over the past twenty years and the recent publication of design codes and guidelines at a national level led the fib (Federation International du Baton) to introduce FRC in the updated version of the CEB-FIP Model Code 90, with the aim of providing a tool for the design of FRC structural elements (Vandewalle, 2010). The fib Model Code proposes two models for the tensile behavior of FRC: the rigid-plastic and the linear-elastic behavior (see Fig. 4). These models are presented in terms of simplified σ-w constitutive laws and reproduce materials with hardening and softening behavior.

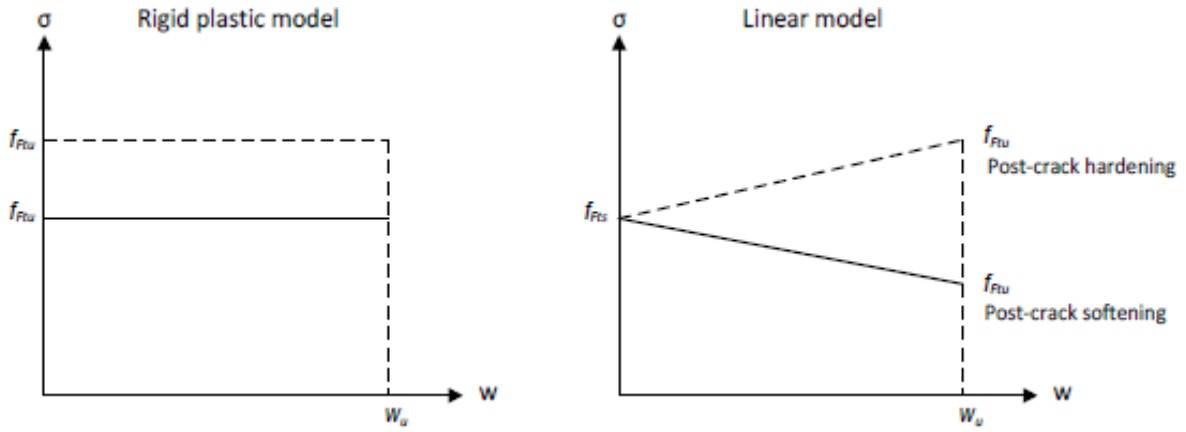

Fig. 4. Simplified constitutive laws (σ-w): a) Rigid-plastic and b) linear-elastic.

The parameters in both diagrams are defined by means of residual flexural tensile strengths, determined in the 3-point bending test EN 14651:2005 (Blanco A. P., 2013). The parameter ts represents the serviceability residual strength defined as the post-cracking strength for crack openings at SLS. On the other hand, f_{tu} represents the ultimate residual strength associated to the ULS crack opening w_u, which is the maximum crack opening accepted in structural design. For the rigid-plastic model the value of w_u is 2.5 mm, whereas for the linear-elastic model it depends on the ductility required. The equations to determine the parameters fts and f_{tu} are presented in Table 1. Since these two models are simplifications, the fib Model Code recommends the use of more advanced constitutive laws for numerical analysis (including the first crack tensile strength) (Blanco A. P., 2013).

In order to define the stress-strain constitutive laws (σ-ε) it is necessary to distinguish between softening materials and hardening materials. A material is regarded as strain hardening if it shows hardening behavior in tension up to an ultimate strain ε_{Fu}=1%.

Otherwise the material is considered as strain softening.

For softening materials, the σ-ε law is defined by identifying the crack width and the corresponding structural characteristic length (lcs) of the structural element. Hence, the strain can be expressed as ε=w/lcs. The characteristic length l_{cs} is evaluated as:

$$l_{cs} = min\{s_{rm}, y\}$$

The parameter srm is the average crack spacing and y is the distance between the neutral axis and the tensile side of the cross section. In the case of elements with conventional reinforcement, y is evaluated in the cracked phase assuming no tensile strength of the FRC and a load configuration corresponding to the SLS of crack opening and crack spacing (see Fig. 5a). In sections without traditional reinforcement under bending or under combined tensile-flexural and compressive-flexural forces with the resulting force external to the section, the value of y is assumed equal to the height of the section (see Fig. 5b). Notice that the use of the characteristic length is not necessary for hardening materials.

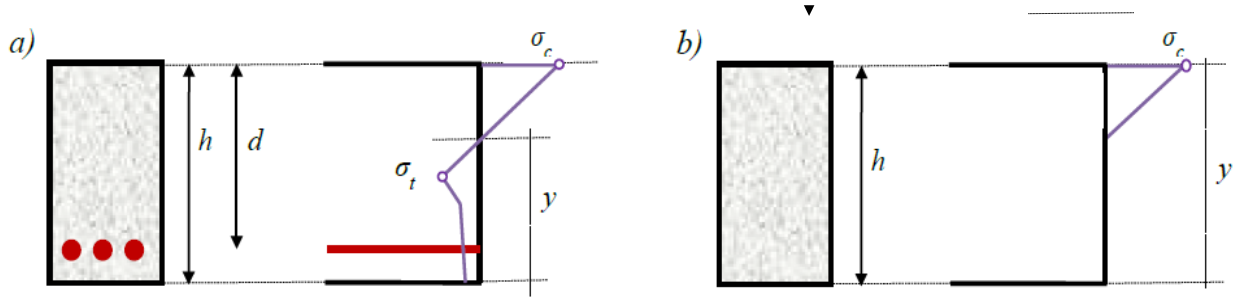

Figure 6:Definition of the parameter "y" for a) sections with traditional reinforcement and b) section without traditional reinforcement. (Blanco A. P., 2013)

Once introduced the concept of characteristic length, it is important to remark that the the ultimate crack width w_u required to estimate f may be calculated as $w_u=l_{cs}\cdot\varepsilon$. The ultimate strain ε equals 2% for variable strain distribution along the cross section and 1% for tensile strain distribution along the cross section. This is valid for softening or hardening materials.
The resulting σ-ε relations are presented in Table 1 (Blanco A. P., 2013). For materials with a softening behavior, the second branch suggested in the pre-cracking stage corresponds to the constitutive law for plain concrete until the intersection between the residual post- cracking behavior and the unstable crack propagation occurs. This stretch is indicated as "MC90 Plain concrete" in Table 1. If the intersection does not occur due to the hardening behavior of the material, another branch is proposed

Regarding the characterization of the tensile behavior, although the bending test EN 14651:2005 (Blanco, 2013) is recommended, other tests may be accepted if proven correlation factors with the parameters of EN 14651:2005 are used. In this sense, the fib Model Code advises not to use uniaxial tensile tests for standard testing of new mixtures due to the associated difficulty of execution and interpretation. Additionally, a proper consideration of the long-term behavior of cracked FRC under tension is required for those structural fibers whose long-term performance is influenced by creep (such as organic or natural fibers). Following the example set by the CNR-DT 204 (Blanco, 2013) and EHE-08 [5], the fib Model Code specifies that fiber reinforcement can partially or totally substitute conventional reinforcement at ULS if certain requirements about the characteristic residual strengths and the limit of proportionality (as defined in EN 14651) are fulfilled.

The Model Code also presents partial safety factors for materials and an orientation factor (K) for the design. This factor equals 1 if an isotropic fiber distribution is assumed and may be lower or higher than 1 if favorable or unfavorable effects are experimentally verified. This is a rather innovative approach since none of the previous guidelines accounted for the influence of fiber orientation due to casting, compaction or concrete consistency in the design. Moreover the Model Code is the first to suggest the execution of special tests to determine the effect of fiber orientation in structural specimens that are representative of the material in the structural element (Blanco, 2013)

1.6 Modelling of Steel Fibre Reinforced Concrete Beams with Bar Reinforcement

The majority of studies on SFRC have been concentrating on members containing steel fibres only, while in most practical applications of SFRC construction, structural members are reinforced both with SFRC and steel bar reinforcement. A combination of steel fibres and tensile reinforcing bars can bring together the advantages of both: the reinforcing bars carry the forces in the tension chord, while the steel fibres provide a confinement of the concrete cover, prevent spalling and carry multiaxial loads (Meškėnas A. , 2018).

The derived material models of tensile SFRC, determined through standard test methods, are suitable for deformation analysis of SFRC elements without bars. However, their adequacy for the modelling applications of the deformation and cracking behavior of SFRC elements with bar reinforcement still remains an issue and results in substantial errors (Meškėnas A. , 2018).

A number of theoretical models have been proposed to predict serviceability behavior of concrete elements with bar reinforcement. These models may be subdivided into such categories: stress-transfer approaches, fracture mechanics models and average stress-average strain approaches (Gribniak et al. 2013b). For the analysis of serviceability limit state, models based on stress-transfer (also called force transfer, or partial interaction) approach appear to be a reasonable alternative to commonly used code techniques, as it realistically predicts the

cracking behavior of reinforced concrete, bond-slip mechanics and the effect of tension stiffening (Jakubovskis et al. 2013, Sokolov et al. 2016) (Meškėnas A. , 2018) .

When steel fibre and bar reinforcement are combined, the post cracking tensile capacity of the SFRC should be taken into account when calculating crack widths and spacing for the elements with bar reinforcement. In traditionally rein- forced concrete members the crack width depends on the distance between cracks,

i.e. crack spacing, and the distance between cracks is determined by the bond length of the reinforcing bars. At a crack section the tensile force in the plain concrete is zero with all the tensile force being carried by the steel bar reinforcement. Further from the crack the reinforcing bars bonded into the concrete matrix transfer tensile force into the concrete, with all the force being transferred into the concrete at a distance equal to the reinforcing bars development length. This dis- tance in this research will be called as stress-transfer length ltr. The minimum spacing between cracks is assumed to be equal to one stress-transfer length and the maximum spacing is two stress-transfer lengths. The maximum crack width will therefore result when the cracks are spaced at the maximum spacing of two development lengths. When bar reinforcement is combined with fibres bridging the crack the transmitted tensile stress across the crack is shared between the re- inforcing bars and the fibres. This results in the smaller tensile force in the con- ventional reinforcement at the crack and, thus, the stress-transfer length of the steel is decreased. Reducing the stress-transfer length and the strain of the reinforcement decreases the crack spacing and, consequently, results in more cracks but with a smaller width (Fischer & Li 2002, Deluce et al. 2014).

The essential aspect considering the stress-transfer models is the reinforcement bond-slip model used for analysis. A detailed survey of existing literature about the bond of ribbed reinforcing steel bars embedded in SFRC was carried out by Bigaj-van Vliet (2001), Dupont et al. (2002) and Plizzari et al. (2002). How- ever, the existing studies on the effect of steel fibres on the bond behaviour of ribbed bars in concrete reported contradictory results. The performed studies are hardly comparable due to variations in mechanical and geometrical properties of the bar, steel fibre and concrete matrix properties. Therefore, up to present time, there is no clear agreement regarding the effect fibres to the overall bond-slip relationship.

The research performed by Cholmianskij (1981), Salem & Maekawa (1999), Ruiz et al. (2007) shows that due to the damage of concrete close to the crack section bond deterioration occurs. Bond stress is rapidly reducing and is equal to zero in the section of the crack. The parts affected by the damage of the bond are further called as the damage zone. A number of damage zone

models defined in the literature (Jakubovskis et al. 2013, Jakubovskis & Juknys 2016) show that the length of the damage zone is related to the diameter of the steel bar reinforcement

as well as the load level. The stress-transfer model developed in this thesis con- siders the bond-slip relationship given in Model Code 2010 (fib 2013). According to the Model Code 2010, the length of the damage zone is taken ld = 5. Within the length of the damage zone, the bond stresses are defined as:(1.18) Here λ is the bond reduction factor. The Model Code 2010 assumes that λ in- creases linearly from 0 in the crack to 1 in the end of the damage zone.

1.7 REVIEW OF DEFLECTION STUDIES OF REINFORCED CONCRETE BEAMS

During the service period of the structure, various loads will generate different deformations, such as mid-span deflections of beams and slabs. The main material used in reinforced concrete structures is concrete, which has a low strength and large cross-sectional dimensions of the elements. At the same time, the integrity of the joints and interconnections of the concrete structure is strong, so it has greater stiffness and less deformation.

With the further development of concrete structure, the two materials, steel and concrete, have changed considerably. Thanks to various high-efficiency admixtures, the improvement of cement quality and concrete production process, high-strength concrete has higher compressive strength and deformation resistance than ordinary concrete. However, high-strength concrete exhibits a great deal of brittleness and its ultimate strain is also lower than that of ordinary concrete. On the other hand, the use of high-strength steel bars reduces the reinforcement ratio of reinforced concrete members and saves steel, but it also causes the stress of reinforced concrete members to increase under the serviceability limit state. These conditions increase the deformation of the elements under load, especially after concrete cracking, and excessive deformation can affect the performance and even the safety of the structure.

Excessive deformation of members may have adverse effects on structural engineering **[2]**:

1) Change the internal force or bearing capacity of the structure. For example, the additional eccentricity under compression increases, and the bearing capacity decreases; the rigidity of the structure is too small, and the structural response under the action of mechanical equipment

vibration, moving load, or wind vibration is intensified.

2) Affect the use function of the building. For example, the deformation of the seam structure of the multistory plant is too large, which affects the operation accuracy of precision instruments and the machining accuracy of precision machine tools; the deformation of the crane beam affects the normal operation of the crane and the period of use; the deformation of the roofing components is too large, tearing the waterproof layer, sagging of the components, water accumulation on the surface and water seepage.

3) Causes damage to connected building components. Examples include sagging and cracking of ceilings and roofs, local damage and cracking of supported lightweight partitions, and obstruction of opening of doors, windows and movable partitions.

4) Causes a sense of psychological insecurity. For example, the sagging and bending of beams and slabs, the lateral deflection of columns and the trembling of thin slabs can all cause psychological panic. Sometimes this factor plays a dominant role and even if the safety and performance of the structure is not a problem, measures have to be taken to address it.

Therefore, for the deformation of concrete structures, many design codes and some safety provisions of similar design codes stipulate the maximum limits of deflection. The American code (ACI 318-19, 2019) then limits the deflection of members to 1/180 to 1/480 of the calculated length, $\boldsymbol{L_0}$, or the absolute value of the deflection, as well as limiting the angle of inclination (radian) of columns and walls, depending on the working conditions of the member. Eurocode2 has two regulations on deflection: (1) To avoid possible damage to the appearance and function of the structure, the deflection should not exceed 1/250 of the calculated length, $\boldsymbol{L_0}$ for beams, slabs or cantilevered members subjected to quasi-permanent loads. part or all of the deflection may be offset by arching, but the arch should not exceed 1/250 of the calculated length, $\boldsymbol{L_0}$. (2) Deflections that damage adjacent structural structures should be limited. For completed structures, deflections under quasi-permanent loads are limited to 1/500 of the calculated length, $\boldsymbol{L_0}$. Depending on the sensitivity of the adjacent parts, other limits may also be considered.

The deflection of flexural members under short-term loads is fundamental to the problem of deflection of reinforced concrete members. It is known from structural mechanics that the formulae for calculating the deflection of homogeneous elastomeric bars are based on the following relations: (1) physical relations - Hooke's law; (2) equilibrium conditions; (3) geometrical relations - plane section assumption, strain and deflection (curvature) relations. The methods for calculating

the deformation of reinforced concrete members at all stages before yielding are based on this and take into account the non-linear character of the concrete stress-strain relationship in terms of the physical relations.

1.7.1 Review of research on the flexural stiffness of reinforced concrete members

Important research into the flexural stiffness of reinforced concrete members has been carried out early in the world, both experimentally and theoretically. Early research focused on the differences in short-term stiffness of concrete members before and after cracking and the effect of reinforcement ratio on deformation, but the studies were conceptual in nature and no precise quantitative analysis was carried out.

Early scholars, such as Humphrey and Losse in 1911 **[6]**, conducted some experiments on the stiffness of beams, and came to the conclusion that concrete cracking has a great influence on the stiffness, but did not describe the degree of influence of cracking on the stiffness. In 1941, C. Cox **[7]** obtained three stages of load-deflection curves for beams based on the results of tests on 110 beams of rectangular section (including 4 concrete strengths and 23 reinforcement ratios) and found that deformations developed more rapidly in beams with low reinforcement ratios than in beams with high reinforcement ratios.

With the wide application of concrete materials and the surge in the service period of concrete structures, people gradually found that the deformation of concrete components will gradually increase (creep) with the passage of time under the condition of constant load. Therefore, more scholars have focused on the effect of long-term loading on the deformation of concrete structures. Studies by Faber between 1927 and 1932, Ernst and Gilkey in 1935 and many others have demonstrated the order of magnitude of long-term deformation and discussed the effect of the reinforcement rate of reinforcement in the compression zone on the long-term deformation of concrete beams. It was found that the long-term deformation of concrete beams could be significantly reduced by the reinforcement in the compression zone. Washa and Fluck conducted two-year loading experiments on 34 reinforced concrete beams from 1952 and found that the long-term deformation of the flexural members was roughly one to twice the short-term deformation.

Since the 1960s, scholars from all over the world have conducted a deeper analysis and discussion on the short-term and long-term stiffness of concrete flexural members, and constantly

summed up the factors that may affect the stiffness of the members. On the basis of predecessors, the methods and ideas of theoretical research are continuously improved.

Winter [10**]** proposed two methods of calculating short-term stiffness and two methods of calculating long-term stiffness in 1960. They verified their equations with 175 groups of test data collected and obtained more satisfactory results.

Based on the above mentioned studies, Branson proposed a modified effective moment of inertia method for calculating the deflection of reinforced concrete bending members, which is the best known model in the West. At the same time, he also proposed the calculation formula of shrinkage and creep, and summarized these several stiffness calculation methods **[12]**, and corrected the deficiencies in the ACI Code. He proposed the concept of the effective moment of inertia, I_e, which has been used until 2019, and ACI 318-19 [13] adopted an alternative formula for calculating the effective moment of inertia, I_e. In the same year, Hajnal-Konyi [14] analyzed 12 beams that had been loaded for more than two years and found that beam stiffness was affected by high span ratio and reinforcement stress.

Since the 1970s, due to the need for engineering applications, some scholars have started to analyses and study the deformation performance and stiffness of precast floor slabs, continuous box girders of bridges and lightweight concrete beams under the long-term action of loads, and have proposed certain amendments to the theories of the time.

In 1970, Hollington [15] conducted a study on the deformation of prefabricated floor slabs, and found that the effect of arranging steel bars in the compression zone on the long-term deformation reduction of lightweight concrete members was not as good as that calculated by the British Code and ACI Code at that time. In 1971, Pauw [16] found, through a study of a continuous box girder bridge, that long-term deformation was two to three times greater than short-term deformation. The role of K_r (deformation reduction factor) and reinforcement in the compression zone was also revisited. In 1973, Heiman [17] compared the deformation of lightweight concrete beams under design loads, serviceability loads and test loads. He used a different method of long-term load loading from that used by previous scholars (a smaller live load was used to apply the long-term load).

Research on the stiffness of flexural members in China started late, with the main research work being carried out by the Nanjing Institute of Technology (now Southeast University) from the 1960s, but a group of scholars from the Nanjing Institute of Technology had already started

theoretical studies and data preparation in the mid-1950s. A total of about 550 specimens have been tested. The experimental study of cracking and stiffness of reinforced concrete flexural and eccentric members (in tension and compression) with various commonly used sections (including rectangular, T-shaped, inverted T-shaped, I-beam and thin-web I-beam sections with concentrated reinforcement, and ring sections with distributed reinforcement) has been basically completed, and a complete calculation system has been proposed. In this system, the formulas have a uniform form, the calculations are relatively simple and their results are sufficiently accurate. In addition to plain concrete members, calculations are also included for reinforced ceramic concrete and prestressed concrete as well as for restressed ceramic concrete bending members, and also for biaxially bending members, which were not yet available in foreign sources at the time. In addition to the study of the stiffness under service loads, the ultimate state of the member's In addition to the study of stiffness under service loads, the deformation of members in the limit state is also investigated and the corresponding calculation methods are proposed. The calculation of the full curve of bending moment and curvature is also presented. The study of long-term load tests on flexural members began in December 1965 with nine batches of tests on reinforced concrete members, pre-stressed concrete members with and without cracks, reinforced ceramic concrete, circular section members and pre-stressed ceramic concrete members without cracks. Based on the test results, a practical calculation formula for long-term stiffness that takes into account the effects of creep and shrinkage is proposed, which interfaces well with the short-term stiffness formula and is sufficiently accurate **[18]**.

1.7.2 Theoretical methods for calculating short-term deflections of reinforced concrete beams

Effective moment of inertia method

The moment-curvature relationship was further investigated by Branson [11], who found that the cross-sectional stiffness or moment of inertia of reinforced concrete beams decreases as the value of the bending moment increases. The stiffness E_cI_{ucr} before concrete cracking is its upper limit value; the stiffness E_cI_{cr} after the reinforcement yields and the tensile concrete completely withdraws from work is its lower limit value, as shown in Fig.6:

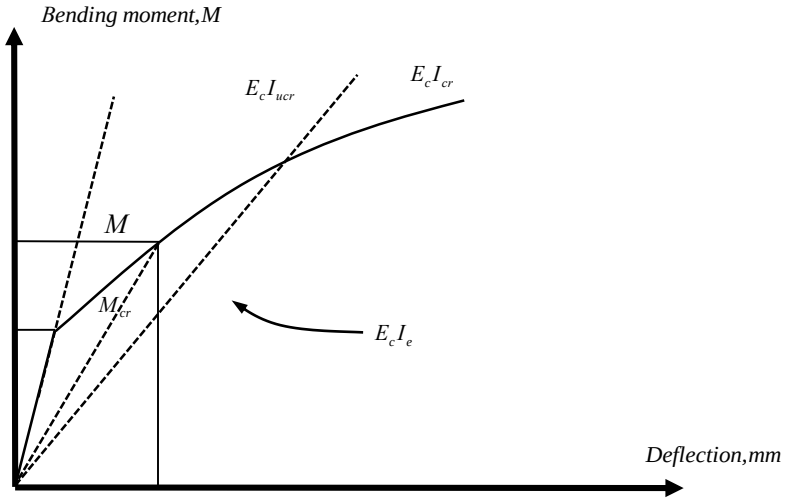

Figure 7:Moment-deflection relations of reinforced concrete beam

When $M>M_{cr}$, the deflection resulting in the beam can be calculated using the effective moment of inertia, I_e :

$$I_e = I_{cr} + (I_g - I_{cr})(\frac{M_{cr}}{M})^m \quad (1.3)$$

$$f = \frac{M}{E_c I_e} \quad (1.4)$$

where

I_{ucr} - the converted moment of inertia of the uncracked section

For the power *m*, setting the power *m* to 4, the tensile contribution of the concrete between the cracks can be considered, giving only the effective stiffness on that section. The average stiffness of the entire span is obtained by setting *m* to be 3, which can reflect the variation of the stiffness *EI* of the beam section along the beam length and the effect of tension hardening of the concrete . ACI 318-14 takes the value of *m* as 3.

2 COMPARATIVE DEFLECTION PREDUCTION DIFFERENT METHODES

2.1 DEFLECTION PREDECTION FOR RC BEAMS

2.1.1 The methods employed

ACI model

The American concrete design code basically follows the effective moment of inertia model proposed by Branson [11]. The model is based on the following four assumptions:

1) Plane section's hypothesis: Under flexural deformation, the cross-section of the member remains planar and the strain in the section has a linear distribution across its depth.

2) The moment of inertia of the uncracked section I_g represents the upper limit of the effective moment of inertia, I_e.

3) Moment of inertia of the fully cracked section I_{cr}, is considered to be the lower limit of the effective moment of inertia, I_e. The latter can never reach I_{cr} value and can only approach it at the advanced load stages.

4) Elastic properties are assumed for both concrete and reinforcement.

The ACI 318-14 recommends the following formula for the effective moment of inertia $\boldsymbol{I_e}$:

$$I_e = \left(\frac{M_{cr}}{M}\right)^3 I_g + \left[1 - \left(\frac{M_{cr}}{M}\right)^3\right] I_{cr} \quad (1.7)$$

The cracking moment M_{cr} is calculated as for the elastic section：

$$M_{cr} = \frac{f_r I_g}{y_t} \quad (1.8)$$

where

y_t - the distance from the tensile surface to the centre of the section (for rectangular section, $y_t = 0.5h$)

f_r - the rupture modulus of concrete

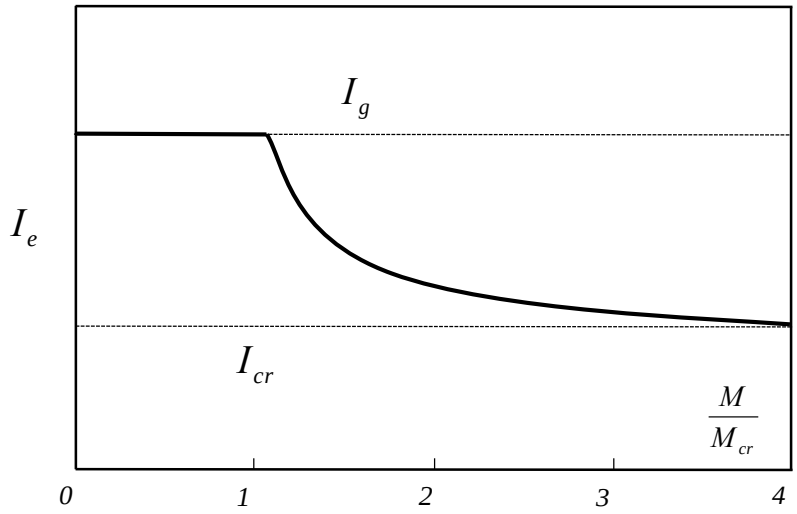

Figure 8:Variation of Ie with moment ratio

The effective moment of inertia given by equation (1.7) is plotted as a function of the ratio M/M_{cr} (equation (1.7) uses the inverse of the bending moment ratio), as shown in Fig. 1.2. It can be seen from Fig. 1.2 that when the maximum bending moment M is less than the cracking moment M_{cr}, that is, M/M_{cr} is less than 1.0, and $I_e=I_g$. As M increases, I_e approaches I_{cr}; and when M/M_{cr} is 3 or more, I_e is almost the same as I_{cr}. The values of M/M_{cr} in the full range of applied loads are 1.5 to 3.

Gribniak et al. [24] and Gilbert [23] showed that Bransons' model significantly underestimates the deflection of reinforced concrete beams with low reinforcement ratios (less than 5%). In order to correct the deflection predictions for reinforced concrete beams with low reinforcement ratios, Bischoff (2005) proposed an alternative relationship for the effective moment of inertia:

$$I_e = \frac{I_{cr}}{1-(\frac{M_{cr}}{M})^2[1-\frac{I_{cr}}{I_g}]} \leq I_g \quad (1.9)$$

Gilbert [25] demonstrated that equation (1.9) predicts deflection for low reinforcement ratio reinforced concrete beams with a significant improvement compared to ACI 318-14. Scanlon and Bischoff [26] then proposed to account for the tensile restraint of concrete due to shrinkage by reducing the value of M_{cr} specified in ACI 318-14 by one third. This method was adopted by ACI 318-19. Therefore, ACI 318-19 recommends the following formula to calculate the effective rotational inertia I_g:

when $\boldsymbol{M} \leq \frac{\boldsymbol{2}}{\boldsymbol{3}} \boldsymbol{M_{cr}}$, $I_e = I_g$

when $\boldsymbol{M} > \frac{\boldsymbol{2}}{\boldsymbol{3}} \boldsymbol{M_{cr}}$, $I_e = \dfrac{I_{cr}}{1 - \left(\dfrac{\left(\frac{2}{3}\right) M_{cr}}{M} \right)^2 \left[1 - \frac{I_{cr}}{I_g} \right]} \leq I_g$ (1.10

Eurocode 2 design code (EC2)

The method used in Eurocode 2 for calculating the stiffness of reinforced concrete flexural members is the bilinear method. In calculating the deformation of concrete sections, assuming two states:

1) uncracked state: reinforcement and concrete are well bonded in tension and compression, and both are in an elastic state.

2) fully cracked state: ignoring the tensile properties of the concrete.

When the tensile stress of the concrete section in the component is less than the tensile strength of the concrete, the component is considered to be in an uncracked state; when the concrete section stress is greater than the tensile strength of the concrete, cracks will occur in the section of the component, and the tensile stress of the concrete between the cracks will be less than the tensile strength of concrete.

Firstly, the curvature of the member in the uncracked and fully cracked state is calculated separately, and then the average curvature in the cracked working state is calculated using the interpolation formula. The equation for the average curvature is as follows:

$$\kappa = (1 - \zeta)\ k_{i1} + \zeta k_{i2} \quad (1.14)$$

$$\xi = 1 - \beta_1 \beta_2 \left(\frac{M_{cr}}{M} \right)^2 \quad (1.15)$$

where

$\boldsymbol{\kappa_{i1}}$ - the instantaneous curvature when the section is not cracked

$\boldsymbol{\kappa_{i2}}$ - the instantaneous curvature when the section is fully cracked

$\boldsymbol{\zeta}$ - the distribution coefficient (when the member is in an uncracked state, $\boldsymbol{\zeta=0.}$)

$\boldsymbol{\beta_1}$ - the coefficient for considering the bonding properties of reinforcement (when the steel bar

is ribbed, β_1=1.0, When the steel bar is smooth, β_1=0.5)

β_2 - the coefficient for considering the type of load (when the load is a short-term load, β_1=1.0, when the load is a long-term, cyclic load, β_2=1.0)

KAKLAUSKAS and SOKOLOV (2021)

INVERSE TECHNIQUE FOR DEVELOPING A CURVATURE MODEL

Kaklauskas and al proposed an inverse technique to derive a tensile-reinforcement model associated with steel from the moment-curvature diagram of a beam. The cross section of the experimental reinforced concrete beam is analyzed according to the geometrical parameters of the experimental beam. For a given material property of a concrete beam, the curvature at a given load is obtained by direct analysis. **Fig. 2.2** show how the tensile-stiffening force is calculated.

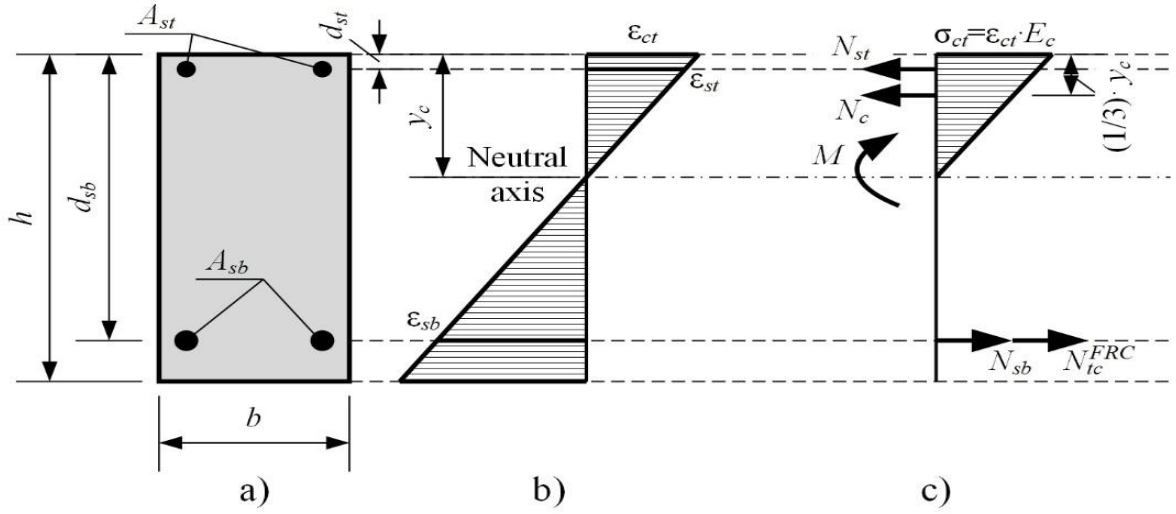

(a).cross-section (b).strain (c).stresses, internal forces, bending moment

Figure 9:Section of a double reinforced beam

Fig. 2.2 (a) shows a cross section of a double reinforced beam, where b and h are the width and height of the section respectively. h_0 is the distance from the upper edge of the concrete compression zone to the center of the combined force of the tensile longitudinal bars and is referred to as the effective height of the section. A_{s1} and A_{s2} are the cross-sectional areas of the reinforcement in the tension and compression zones respectively.

In order to make the results of the analyses carried out Satisfy Branson's approach, the inverse technique satisfies both Branson's hypothesis one and hypothesis four. The inverse technique

satisfies the hypothesis of plane sections, and the concrete and reinforcement are elastic during deformation. So during flexural deformation, the member section remains flat and the strain is distributed linearly along the depth (Fig. 2.2(b)).

The stresses acting in the tensile concrete caused by elasticity, tension stiffening and tension softening are modelled by the resultant tension stiffening force, N_{ts}, termed as the resultant tension stiffening force. The resultant tension stiffening force acts at the centroid of tensile reinforcement, as shown in Fig. 2.2(c). Torres et al. [30] proposed a closed-form computational solution for the calculation of reinforcement-related tensile hardening stresses in flexural RC members, based on Eurocode 2 curvature prediction techniques. From this, the equilibrium equations for the internal forces and bending moments of the tension reinforcements are listed:

$$N_{s1} + N_{ts} - N_c - N_{s2} = 0 \quad (2.1)$$

$$N_c(h_0 - \frac{y_c}{3}) + N_{s2}(h_0 - y_{s2}) - M = 0 \quad (2.2)$$

where

N_{s1} - the internal forces of tensile reinforcement

N_{s2} - the internal forces of compressive reinforcement

N_c - the internal force of compressive concrete

y_c - the distance from the upper edge of the concrete compression zone to the neutral axis

y_{s2} - the distance from the upper edge of the concrete compression zone to the center of the resultant force of the longitudinal reinforcement under compression

Express the internal forces as characteristic strains ($\varepsilon_c, \varepsilon_s, \varepsilon_{cs}$):

$$N_{s1} = \varepsilon_{s1} E_{s1} A_{s1} \quad (2.3)$$

$$N_c = \varepsilon_c E_c \frac{y_c}{2} b \quad (2.4)$$

$$N_{s2} = \varepsilon_{s2} E_{s2} A_{s2} \quad (2.5)$$

where

$\varepsilon_c, \varepsilon_{s1}, \varepsilon_{s2}$ - the strains of the compressive concrete and tensile and compressive reinforcement, respectively.

E_c , E_{s1} , E_{s2} - the modulus of elasticity of the compressive concrete and tensile and compressive reinforcement, respectively.

Replace the internal forces in equation (2.1) and (2.2) with the characteristic strains in equation (2.3), (2.4), (2.5):

$$\varepsilon_{s1}E_{s1}A_{s1} + N_{ts} - \varepsilon_c \frac{E_c y_c b}{2} - \varepsilon_{s2}E_{s2}A_{s2} = 0 \quad (2.6)$$

$$\varepsilon_c \frac{E_c y_c b}{2}(h_0 - \frac{y_c}{3}) + \varepsilon_{c2}E_{s2}(h_0 - y_{s2})A_{s2} - M = 0 \quad (2.7)$$

Based on the assumption of plane sections, the strain can be expressed in terms of curvature：

$$k = \frac{\varepsilon_c}{y_c} = \frac{\varepsilon_{s2}}{y_c - y_{s2}} = \frac{\varepsilon_{s1}}{h_0 - y_c} \quad (2.8)$$

Substituting equation (2.7) and (2.8) into (2.6), the expression for the resultant tension stiffening force is obtained as：

$$N_{ts} = k[\frac{E_c y_c^{\,2} b}{2} + E_{s2}(y_c - y_{s2})A_{s2} - E_{s1}(h_0 - y_c)A_{s1}] \quad (2.9)$$

In equation (2.9), the bending moment, M, and curvature, K, can be obtained by testing, but produce an unknown, the neutral axis depth, y_c. For the calculation of the neutral axis depth, y_c, the moment equilibrium equation can be rearranged into a cubic form (Kaklauskas and Gribniak, **[31]**).

First, expressing the characteristic curvature in terms of curvature, equation (2.7) can be transformed into:

$$k\frac{E_c y_c^{\,2} b}{2}(h_0 - \frac{y_c}{3}) + kE_{s2}(h_0 - y_{s2})(y_c - y_{s2})A_{s2} - M = 0 \quad (2.10)$$

Then, transform Equation (2.10) into a cubic form:

$$-\frac{kE_c b}{6}y_c^{\,3} + \frac{kE_c b h_0}{2}y_c^{\,2} + kE_{s2}A_{s2}(h_0 - y_{s2})\,y_c - kE_{s2}A_{s2}y_{s2}(h_0 - y_{s2}) - M = 0 \quad (2.11)$$

$$C_0 + C_1 y_c + C_2 y_c^{\,2} + C_3 y_c^{\,3} = 0 \quad (2.12)$$

The expressions for the coefficients C_0, C_1, C_2, C_3 can be obtained as follows:

$$C_0 = -kE_{s2}A_{s2}y_{s2}(h_0 - y_{s2}) - M \quad (2.13)$$

$$C_1 = kE_{s2}A_{s2}(h_0 - y_{s2}) \quad (2.14)$$

$$C_2 = \frac{kE_c b h_0}{2} \quad (2.15)$$

$$C_3 = -\frac{kE_c b}{6} \quad (2.16)$$

According to Shengjin's formula, this cubic equation has three roots. Remove the negative root and imaginary root, leaving a real root that satisfies the condition $0 < y_c \leq h_c$:

$$y_c = -\frac{[\,2(C_2^{\,2} - 2C_3C_1)^{0.5}\sin T + C_2\,]}{3C_3} \quad (2.17)$$

$$T = \frac{1}{3}\arcsin[\frac{9C_3C_2C_1 - 27C_3^{\,2}C_0 - 2C_2^{\,3}}{2(C_2^{\,2} - 2C_3C_1)^{1.5}}] \quad (2.18)$$

AN ILLUSTRATION OF INVERSE TECHNIQUE

Six rectangular reinforced concrete beams collected from various experimental programmes were used to illustrate the inverse analysis. The beams were subjected to four-point loading scheme. Main characteristics of the beams are given in Table 4.

Table 4:Main characteristics of RC specimens

Specimen	***h,mm***	***b,mm***	***h_0,mm***	***Φ,mm***	***A_s,mm 2***	***ρ,%***	***f_y,MPa***	***E_s,GPa***	***f_{cu},MPa***
2X16-B30	300	200	260	16	402	0.77	530	20	60.76
S1-2-F10L	305	271	215	18	778	1.05	530	20	60.76
S1-2-F10V	306	277	271	18	798	1.06	530	20	60.76
B3-F-06	302	302	252	12	226	0.3	447	20	35
B-0.5-N3	250	200	215	18	763	1.78	447	20	35
B-0.5-H4	250	200	215	18	102	2.37	540	20	27.96

Table provides the primary geometric and material characteristics, such as section height, reinforcement ratio, effective height, and compressive strength, which are shown within expanded ranges.

The section heights vary between 250 and 350 mm, while the section widths range from 200 to 350 mm. The reinforcement ratios range from 0.3% to 2.37%. The compressive strengths of the concrete range from 20 MPa to 47 MPa.

The test moment – curvature diagrams of the six beams are given in Fig. 10. The calculated tension stiffening forces are presented Fig. 11 where the bending moment is normalized relative to the cracking moment, and the resulting tension stiffening force is represented as Nts/(frbh). The values of fr and Ec needed for the analysis are computed using the ACI 318-19 code.
It can be seen from Fig. 11 that for most of the beams the resultant tension stiffening force reaches zero value at the load level $\boldsymbol{M/M_{cr}} = 3$.

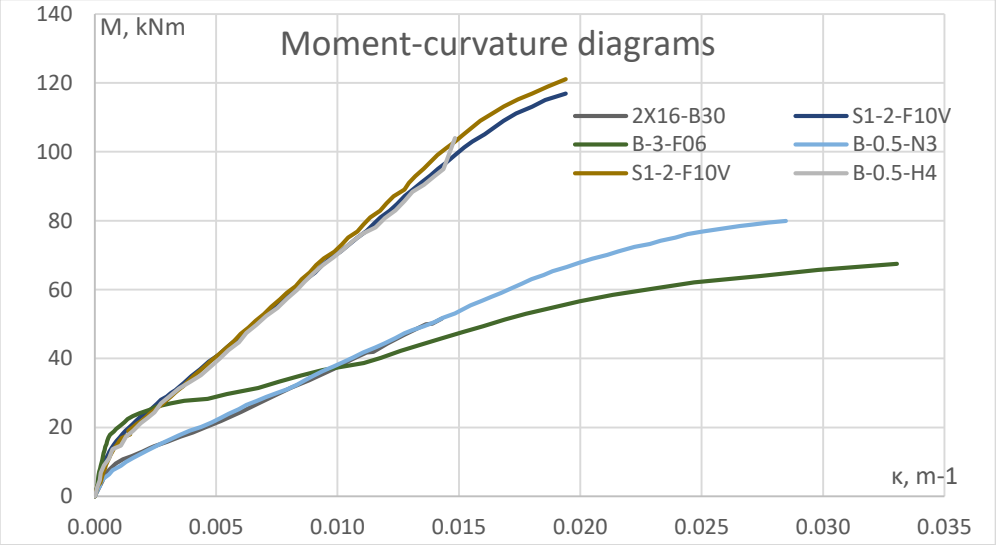

Figure 10:moment-curvature diagrams

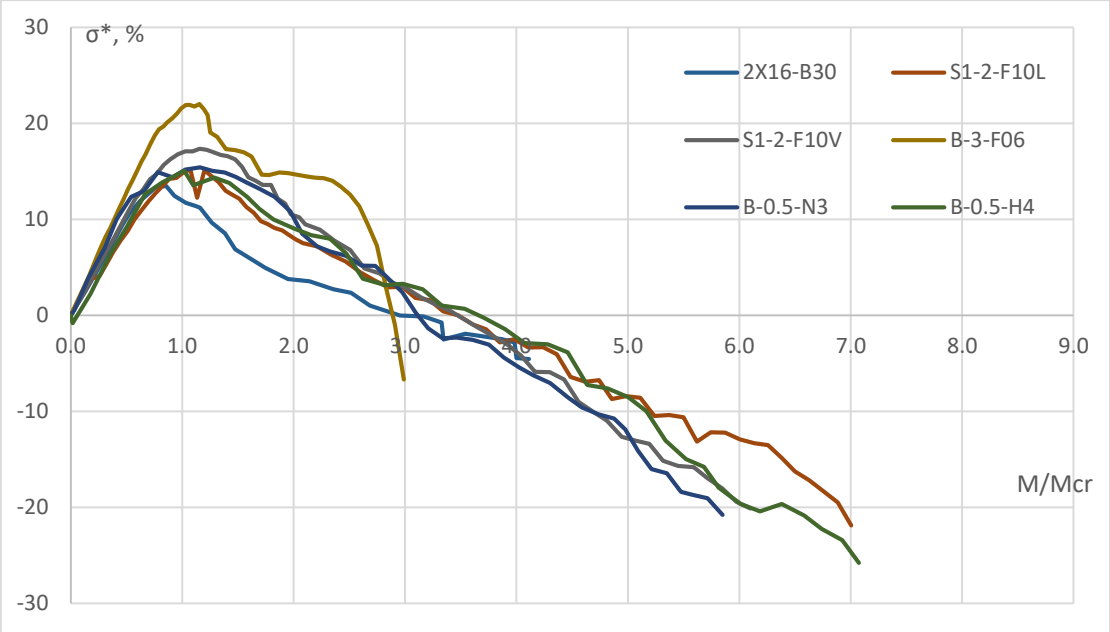

Figure11 : Normalized tension stiffening force for beams with ranging reinforcement ratio,

MOMENT- CURVATURE MODEL FOR RC BEAMS PROPOSED BY KAKLAUSKAS AND SOKOLOV (2021)

The model introduces Assumption 3: The moment of inertia of the reinforced concrete flexural member is equal to I_{cr} when the load level reaches $3M_{cr}$. The model is illustrated in Fig. 10.

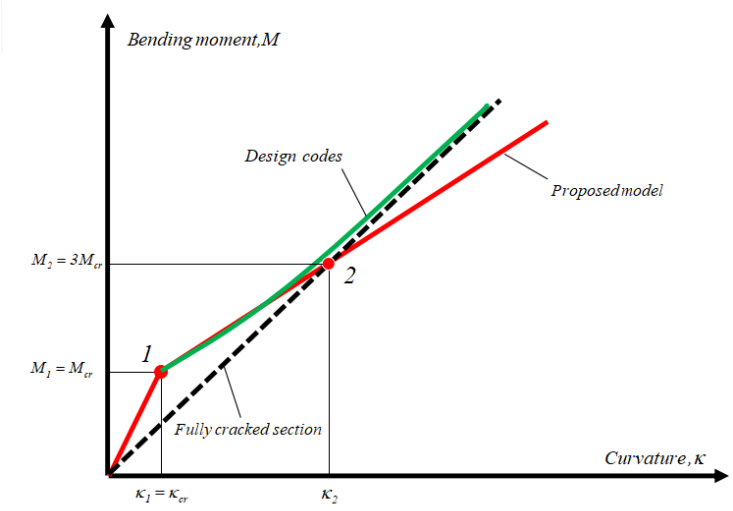

Figure 11:The proposed curvature model proposed by Kaklauskas and Sokolov

Fig. 11 shows a graph of the moment-curvature relationship. Point 1 represents the cracking moment, $M_1=M_{cr}$ and point 2 represents 3 times the cracking moment, $M_2=3M_{cr}$. Following Modified Assumption 3, the bending stiffness of the fully cracked section is assumed to be achieved at bending moment M_2. Based on a linear interpolation between moments M_1 and M_2, the curvature can be calculated from the following expression (Kaklauskas, 2024):

$$\kappa = \kappa_1 + \frac{(\kappa_2 - \kappa_1)(M - M_1)}{(M_2 - M_1)} \quad (2.19)$$

where

$\boldsymbol{\kappa_1}$ - curvature calculated at bending moment $\boldsymbol{M_1}$

$\boldsymbol{\kappa_2}$ - curvature calculated at bending moment $\boldsymbol{M_2}$

Substituting $\boldsymbol{M_2 = 3M_{cr}}$, equation (2.19) can take the following shape：

$$\kappa = \kappa_1 + 0.5(\kappa_2 - \kappa_1)(M / M_1 - 1) \quad (2.20)$$

A simple relationship between deflection and curvature is as follows：

$$f = \kappa s l_0^{\,2} \quad (2.21)$$

So equation (2.20) can be changed from curvature to deflection as follows：

$$f = f_1 + 0.5(f_2 - f_1)(M / M_1 - 1) \quad (2.22)$$

where

$\boldsymbol{f_1}$ - deflection calculated at bending moment $\boldsymbol{M_1}$

$\boldsymbol{f_2}$ - deflection calculated at bending moment $\boldsymbol{M_2}$

Similarly, the curvature can be replaced by the effective moment of inertia, and equation (2.20) can be transformed into an expression based on the effective moment of inertia:

$$I_e = I_1 + 0.5(I_2 - I_1)(M / M_1 - 1) \quad (2.23)$$

Following notations from ACI 318, equation (2.21) takes the form:

$$I_e = I_g + 0.5(I_{cr} - I_g)(M / M_{cr} - 1) \quad (2.24)$$

where

$\boldsymbol{I_1}$ - moment of inertia of uncracked section (ignoring reinforcement), $\boldsymbol{I_1 = I_g}$

$\boldsymbol{I_2}$ - moment of inertia of a fully cracked section, $\boldsymbol{I_2 = I_{cr}}$

Since the results of the curvature analysis depend on the material properties of the concrete, such as the modulus of elasticity, E_c, and the tensile strength, f_c (and possibly also the modulus of rupture, f_r), the characteristic point $M_2 = 3M_{cr}$ uses the same formula as ACI 318 in the curvature analysis.

Equation (2.19) - (2.22) all contain parameters M_1, κ_1, κ_2. The cracking moment M_1 is calculated using the formula of ACI 318:

$$M_1 = M_{cr} = \frac{f_r I_g}{y_t} \quad (2.25)$$

where

$\boldsymbol{y_t}$ - the distance from the centroid of the section to the extreme tension fiber

The curvatures $\boldsymbol{\kappa_1}$ and $\boldsymbol{\kappa_2}$ are represented by the following equations:

$$\kappa_1 = \frac{M_1}{E_c I_1} = \frac{M_{cr}}{E_c I_g} \quad (2.26)$$

$$\kappa_2 = \frac{M_2}{E_c I_2} = \frac{3M_{cr}}{E_c I_{cr}} \quad (2.27)$$

2.1.2 Comparison of predicted and test curvate

The curvature of the experimental beams was compared with the results predicted by the theoretical models. Predictions are expressed in terms of normalized curvature:

$$\bar{k} = \frac{\kappa_{cal}}{\kappa_{exp}}$$

Where,

κ_{cal} - Curvature calculated by new model and code technique

κ_{exp} - Curvature of the experimental beam

In this study, the normalized curvatures are considered to be a random variable. Therefore, the normalized results can be evaluated using statistical methods.

The basic statistical characteristics, the mean ***m***, standard deviation ***SD***, and coefficient of variation ***CV***, were calculated using these formulas.

$$m_{\bar{f}} = \frac{1}{n}\sum_{i=1}^{n} f_i \quad (2.32)$$

$$s_{\bar{f}} = \sqrt{\frac{1}{n-1}\sum_{i=1}^{n}(\bar{f} - m_{\bar{f}})^2} \quad (2.33)$$

$$CV = \frac{s_{\bar{f}}}{m_{\bar{f}}} \quad (2.34)$$

Twenty RC beams having different geometrical and materials characteristics collected from the litearture were used to assess the predictive capabilities of the models discussed. First fourtheen beams were taken from the tests of Clark and Speirs (1978) and the remaining six beams represent

the tests of Figarovski (19952). Main characteristics of the beams, like section height, effective depth, width, reinforcement area, reinforcement ratio, modulus of elasticity of steel and concrete are presented in Table 5.

Table 5:Main characteristic of test members employed in the analysis

Specimen	***h,mm***	***d,mm***	***b,mm***	***Φ,mm***	***A_s,m2***	***ρ,%***	***f_y,MPa***	***E_s,MPa***	***f_{cu},MPa***
B1	0.41	0.38	0.203	25	0.00147	0.02	318.2	206000	27.0
B1R	0.412	0.368	0.202	25	0.00147	0.94	318.2	206000	27.8
B2	0.408	0.363	0.203	20	0.00094	0.93	274.1	206000	26.6
B2R	0.408	0.367	0.204	20	0.00094	0.84	274.1	206000	31.7
B3	0.407	0.373	0.204	16	0.0006	1.46	299.6	206000	30.5
B3R	0.409	0.376	0.204	16	0.0006	0.93	299.6	206000	29.2
B4	0.409	0.379	0.204	12	0.000339	1.48	299.6	206000	23.1
B4R	0.406	0.37	0.204	12	0.00034	1.58	299.6	206000	24.9
B5	0.204	0.167	0.203	16	0.0006	0.67	299.6	206000	23.4
B5R	0.202	0.169	0.202	16	0.0006	0.44	299.6	206000	28.2
B6	0.306	0.268	0.203	16	0.0006	0.70	299.6	206000	21.0
B6R	0.308	0.273	0.203	16	0.0006	0.07	299.6	206000	27.3
B7	0.513	0.48	0.203	16	0.0006	0.12	299.6	206000	18.4
B7R	0.511	0.473	0.204	16	0.0006	0.11	299.6	206000	23.4
P3-2Pd	0.25	0.23	0.18	12	0.00036	0.68	412.0	200000	26.6
P3-1Pd	0.25	0.23	0.18	12	0.00036	0.29	412.0	200000	26.6
P2-2Pk	0.252	0.232	0.179	7	0.0002	0.50	420.8	200000	30.4
P3-1Pk	0.25	0.229	0.18	7	0.00024	0.33	509.1	200000	17.7
P2-2Pd	0.251	0.231	0.179	7	0.0002	0.48	28.7	200000	28.7
P2-1Pk	0.249	0.225	0.18	7	0.00017	0.34	18.6	200000	18.6

The moment – curvature diagrams of the test R/SFRC beams predicted by the three models are shown in Figures 12 to 29. The figures also show the normalized curvature – bending moment moments graphs.

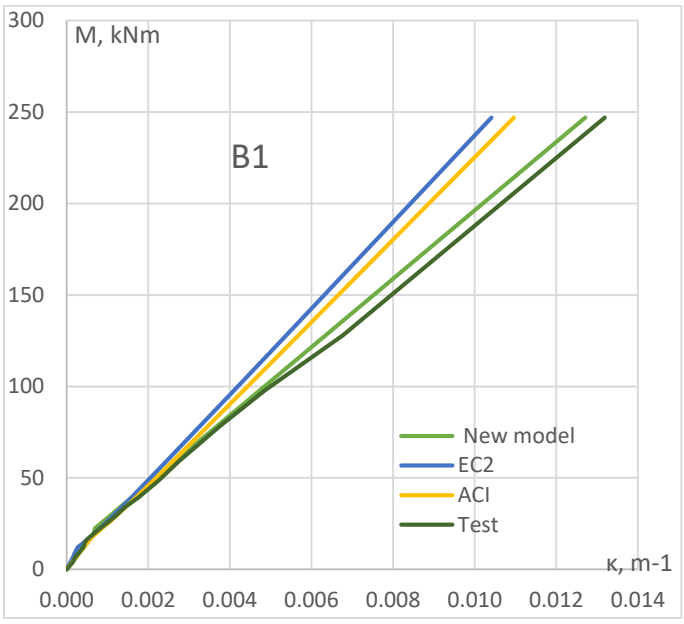

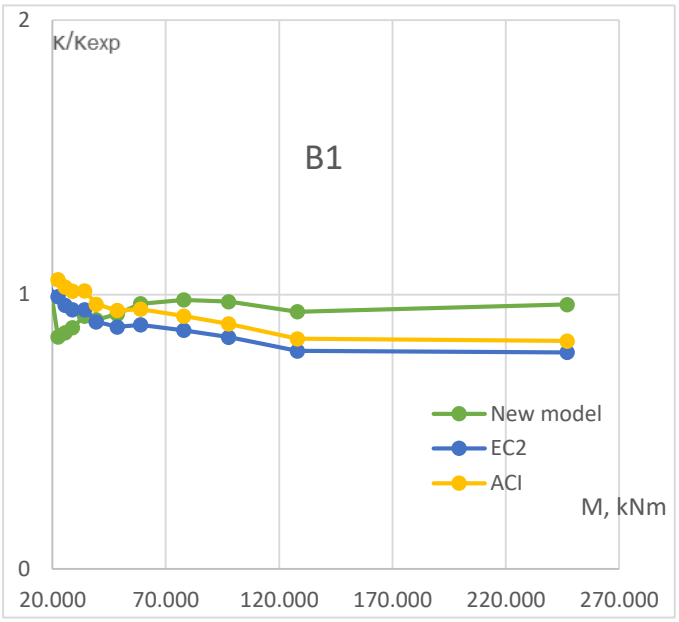

Figure 12:Predicted curvature of test RC beam B1(Clark and Speirs 1978)

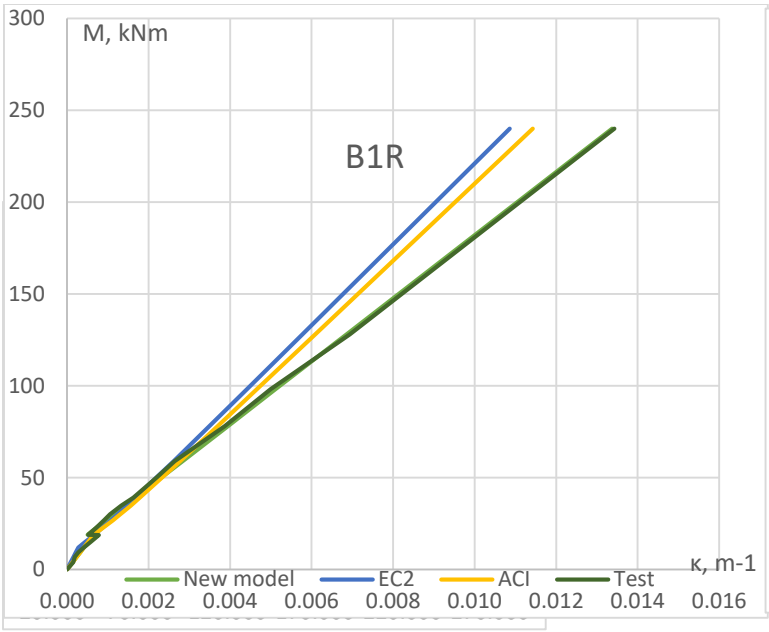

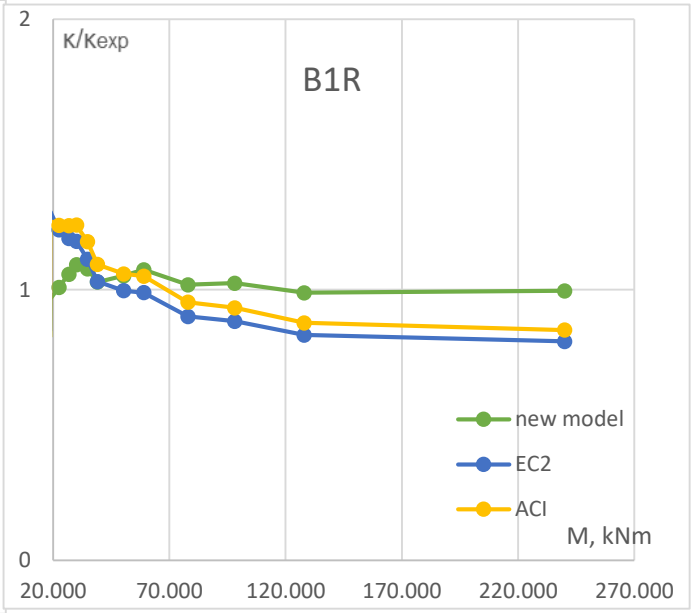

Figure 13:Predicted curvature of test RC beam B1R (Clark and Speirs 1978)

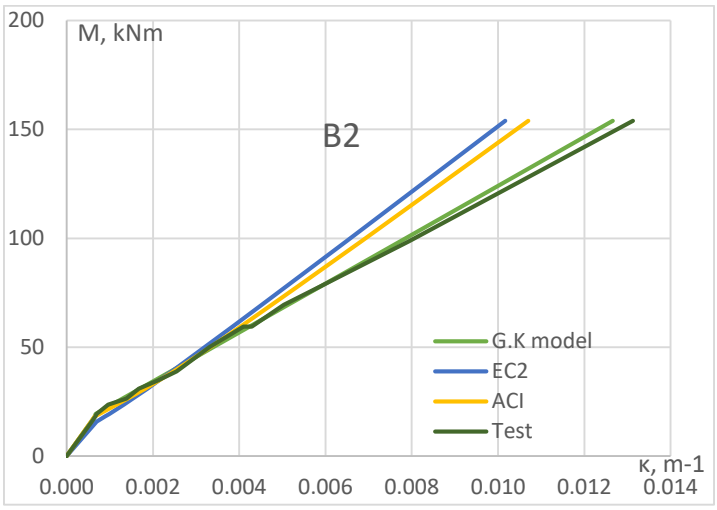

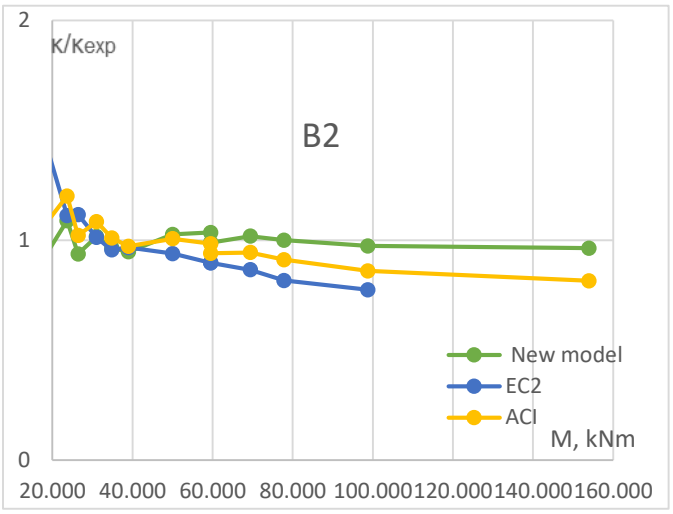

Figure 14:Predicted curvature of test RC beam B2(Clark and Speirs 1978)

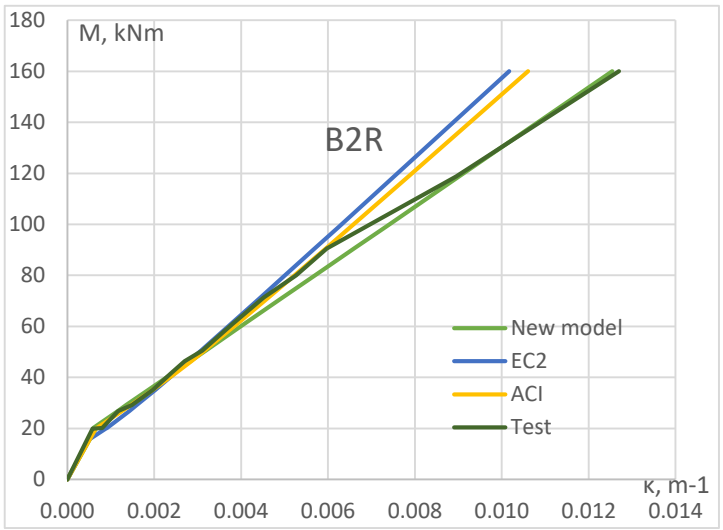

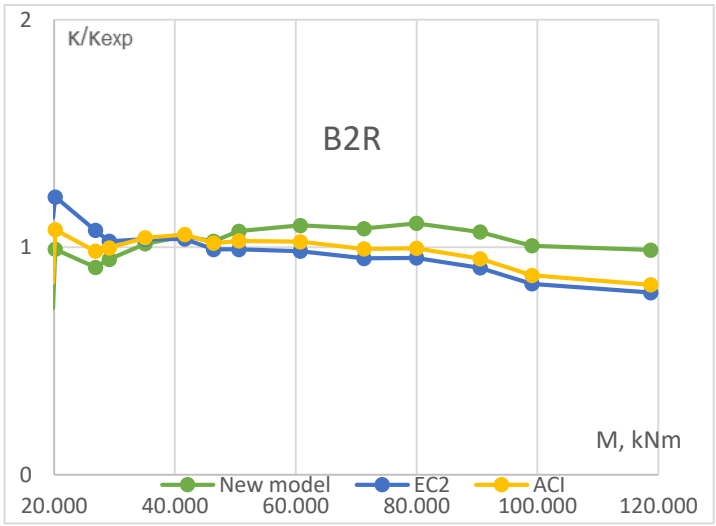

Figure 15:Predicted curvature of test RC beam B2R(Clark and Speirs 1978)

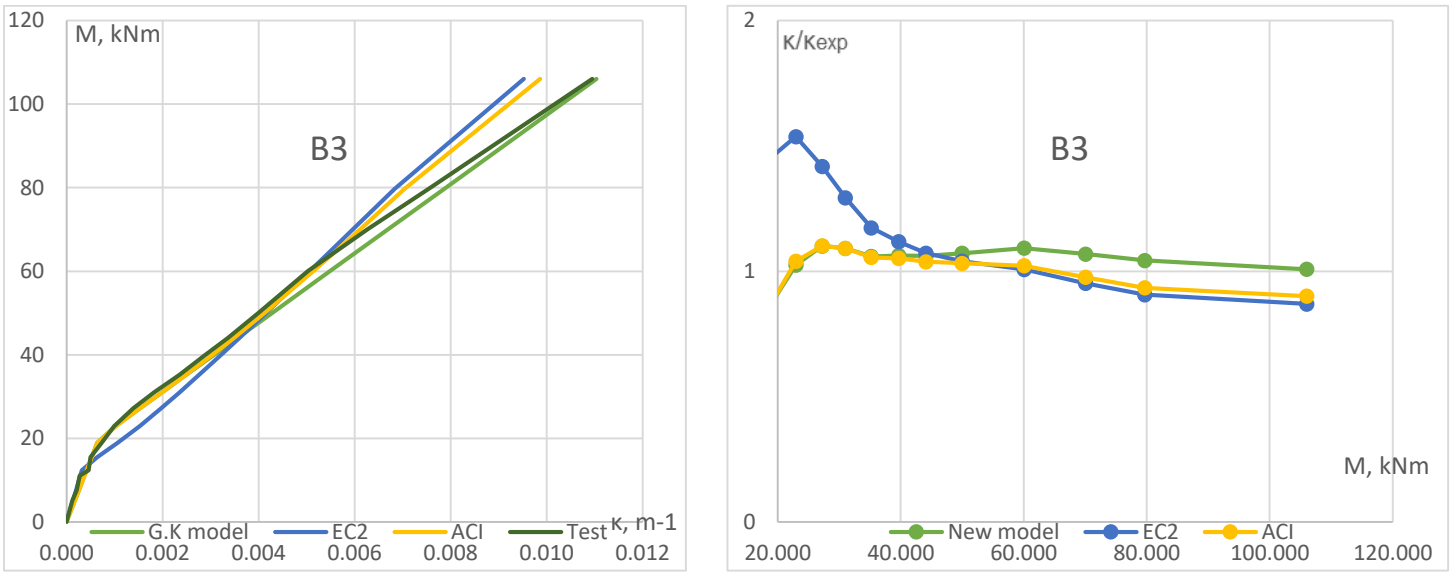

Figure 16:Predicted curvature of test RC beam B3(Clark and Speirs 1978)

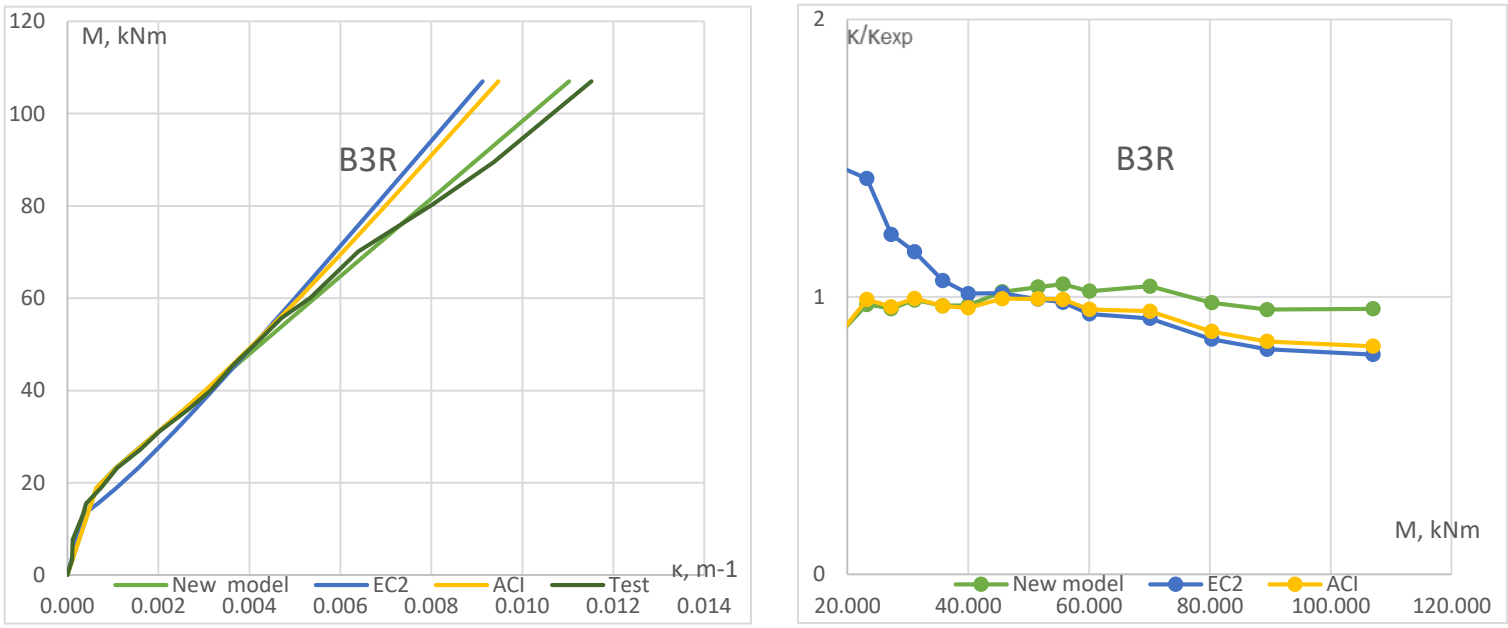

Figure 17:Predicted curvature of test RC beam B3R(Clark and Speirs 1978)

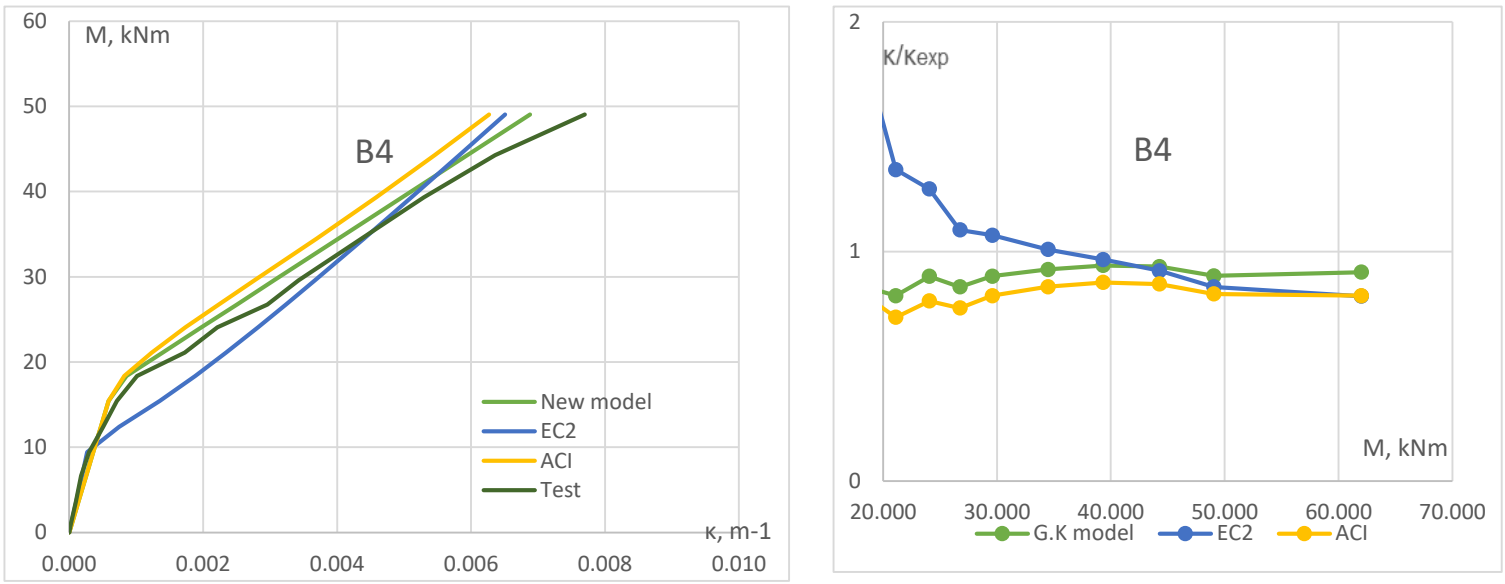

figure 18:Predicted curvature of test RC beam(Clark and Speirs 1978)

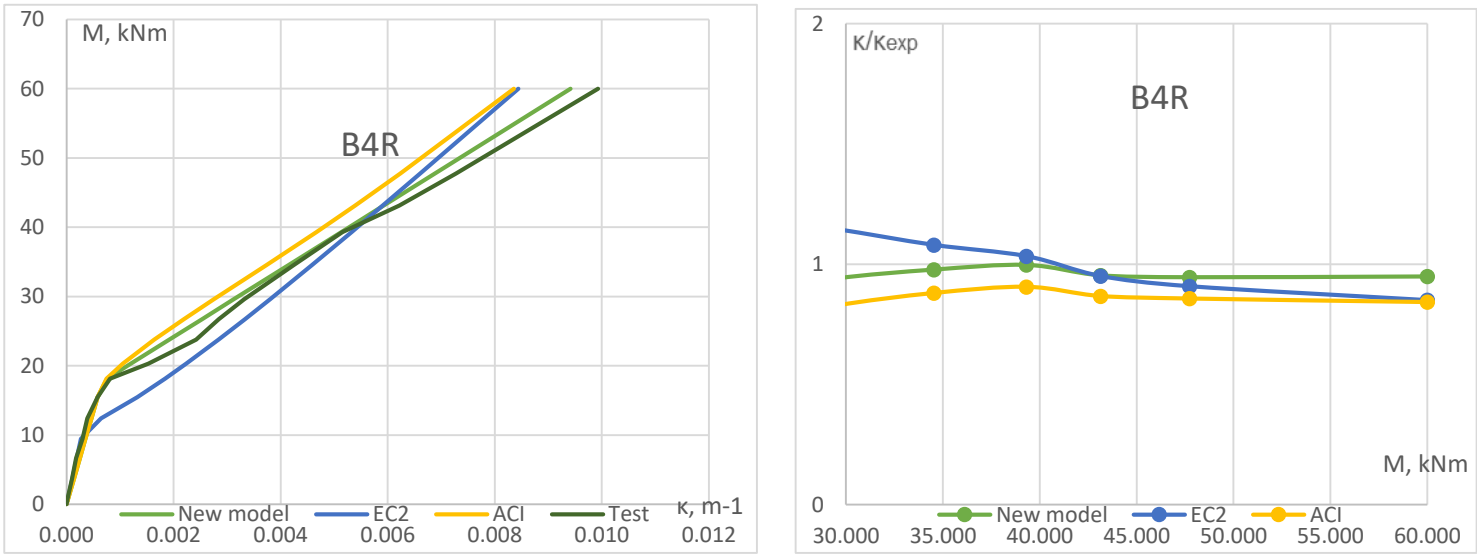

Figure 19:Predicted curvature of test RC beam B4R(Clark and Speirs 1978)

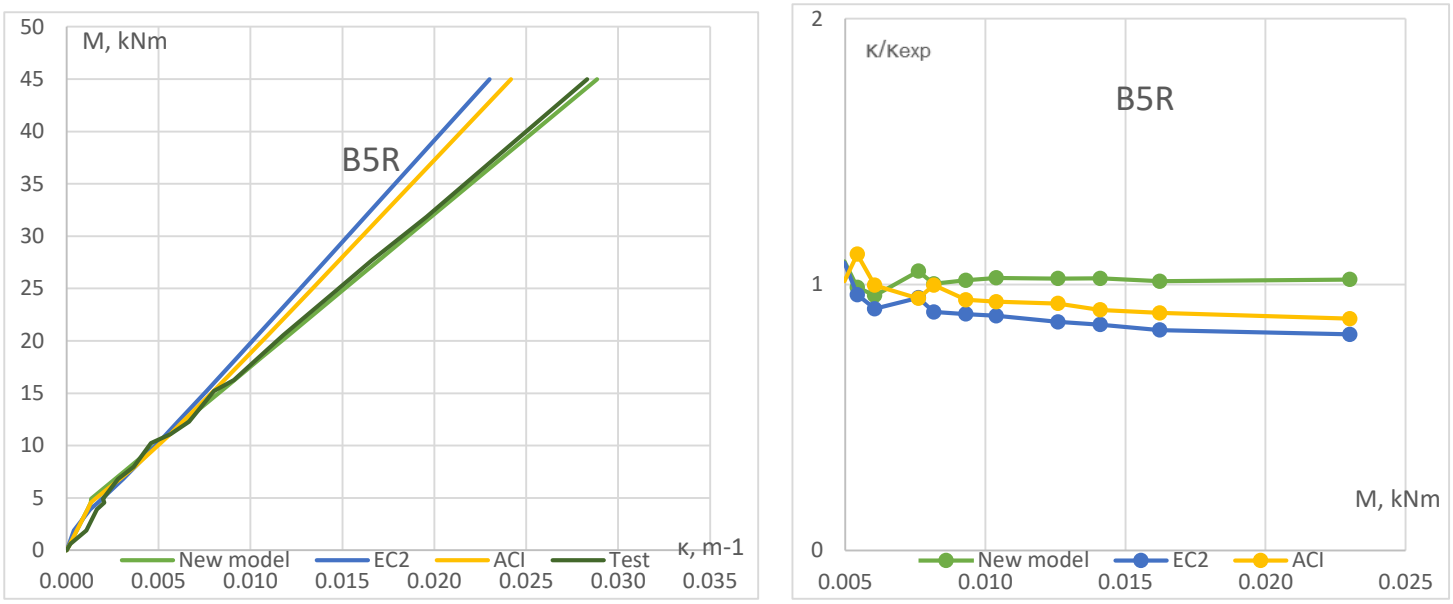

Figure 20:Predicted curvature of test RC beam B5R(Clark and Speirs 1978)

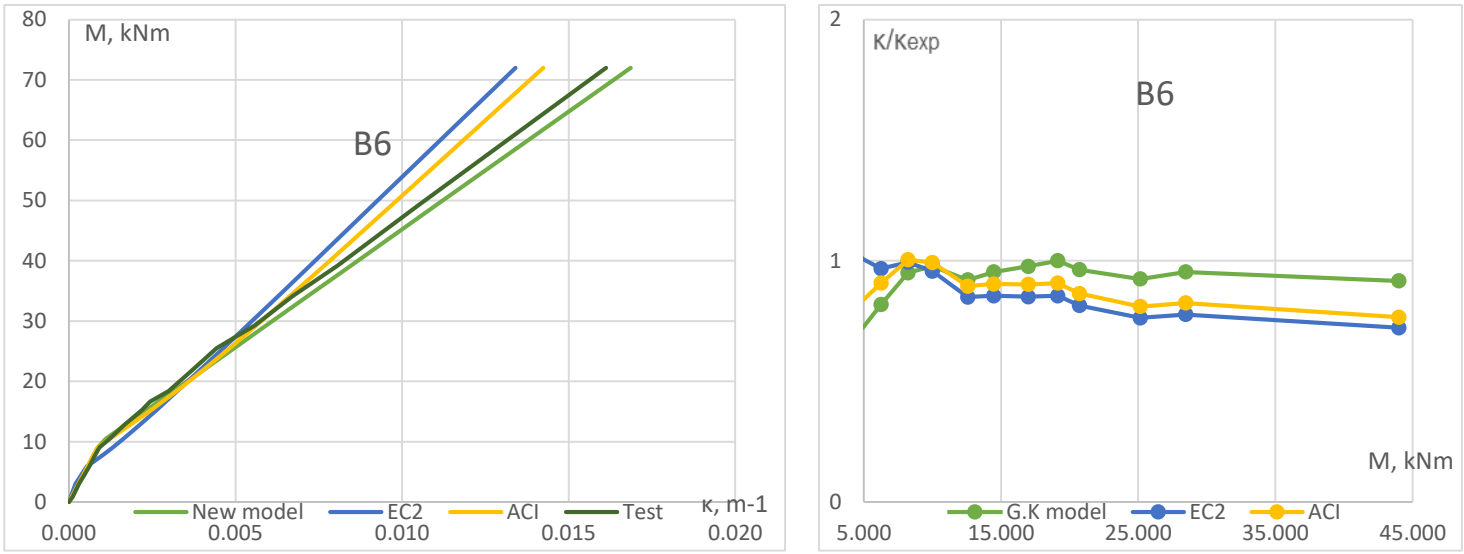

Figure 21:Predicted curvature of test RC beam B6(Clark and Speirs 1978)

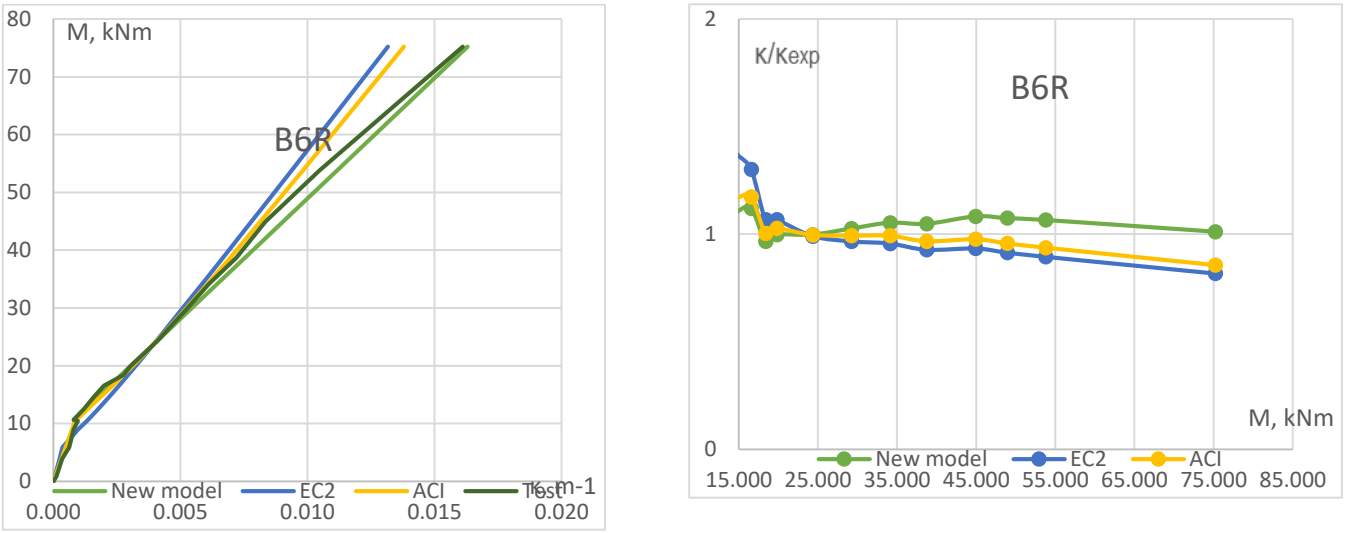

Figure 22:Predicted curvature of test RC beam B6R(Clark and Speirs 1978)

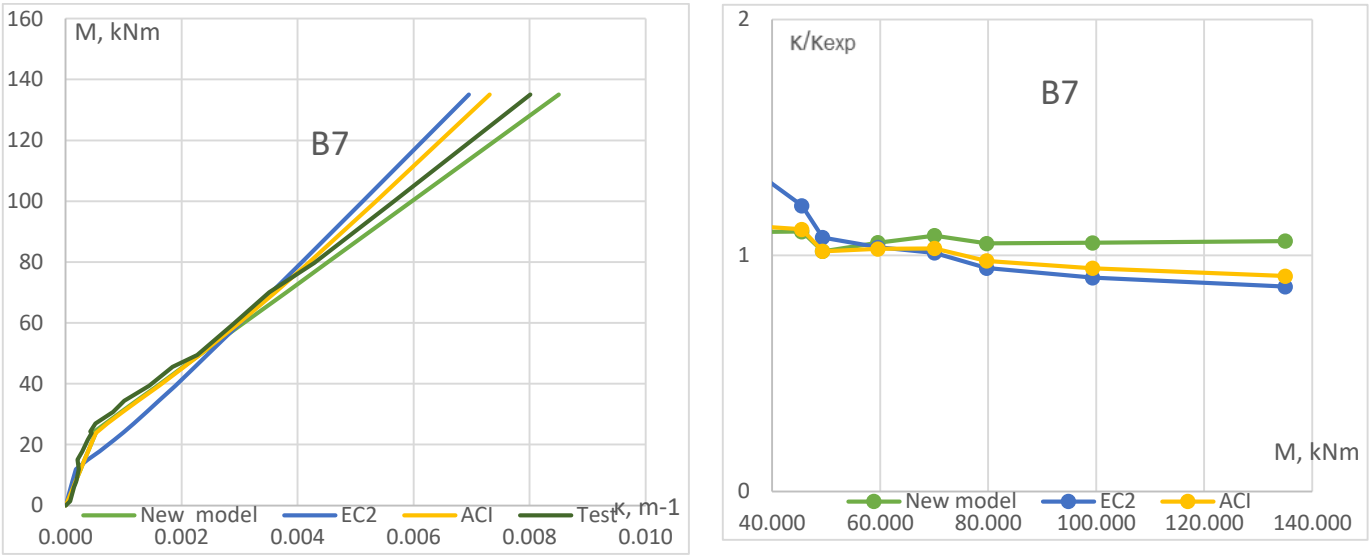

Figure 23:Predicted curvature of test RC beam B7(Clark and Speirs 1978)

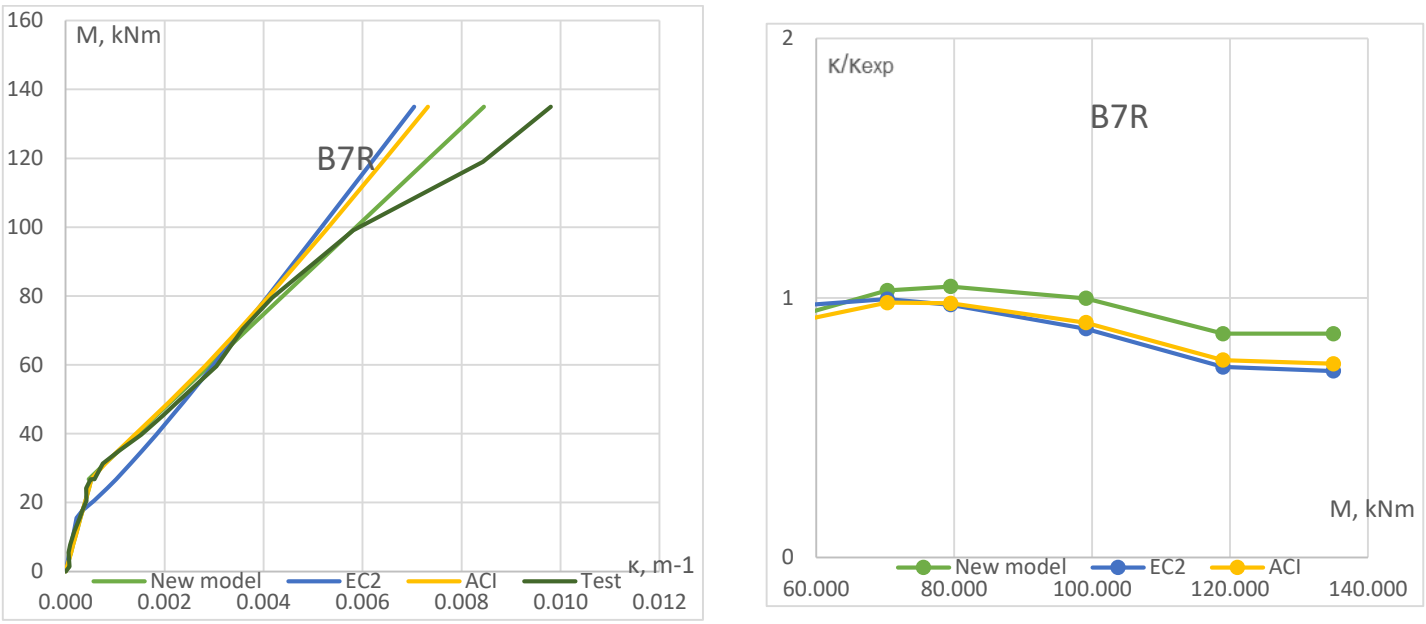

Figure 24:Predicted curvature of test RC beam B7R(Clark and Speirs 1978)

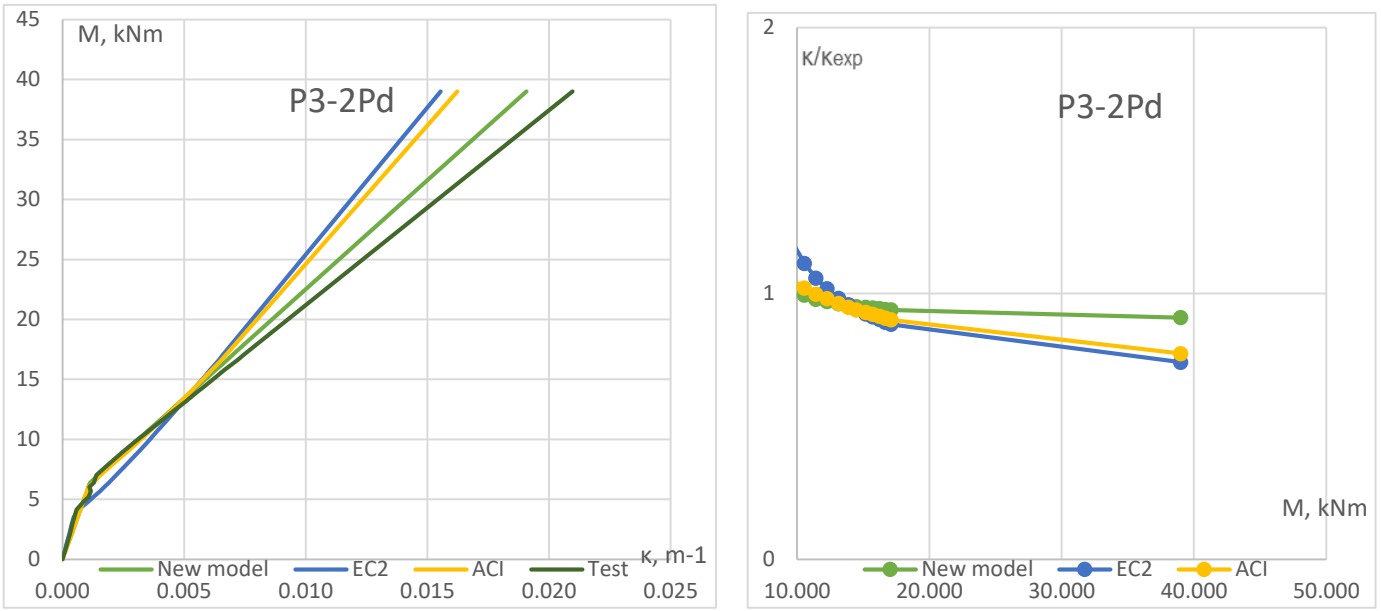

Figure 25:Predicted curvature of test RC beam P3-2Pd(Clark and Speirs 1978)

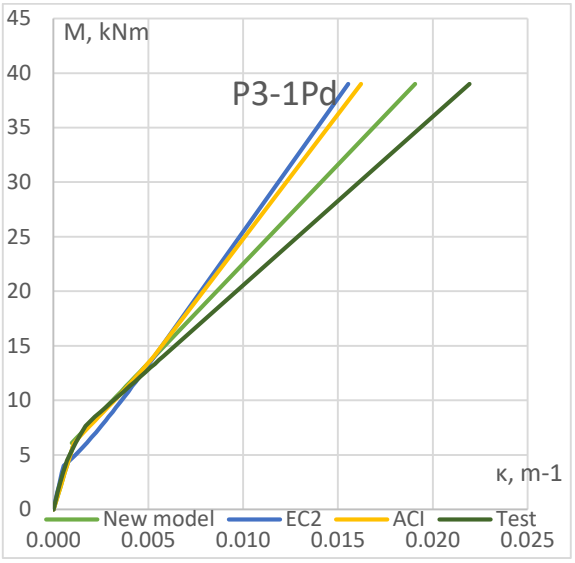

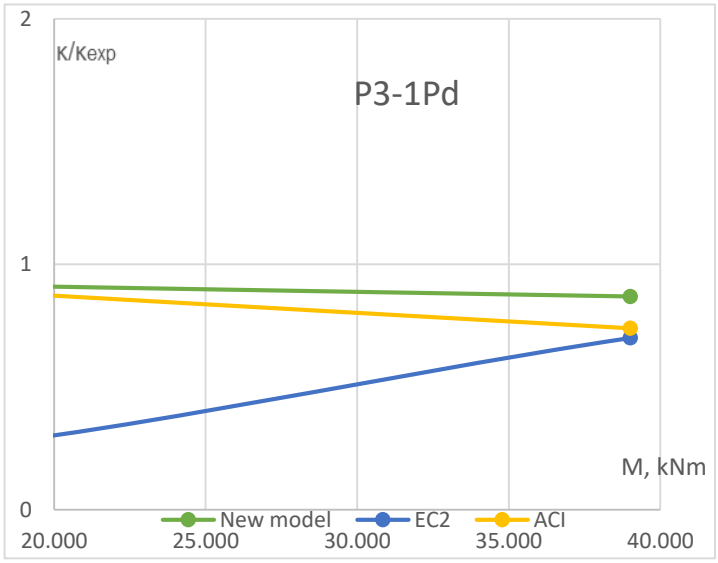

Figure 26:Predicted curvature of test RC beam P3-1Pd

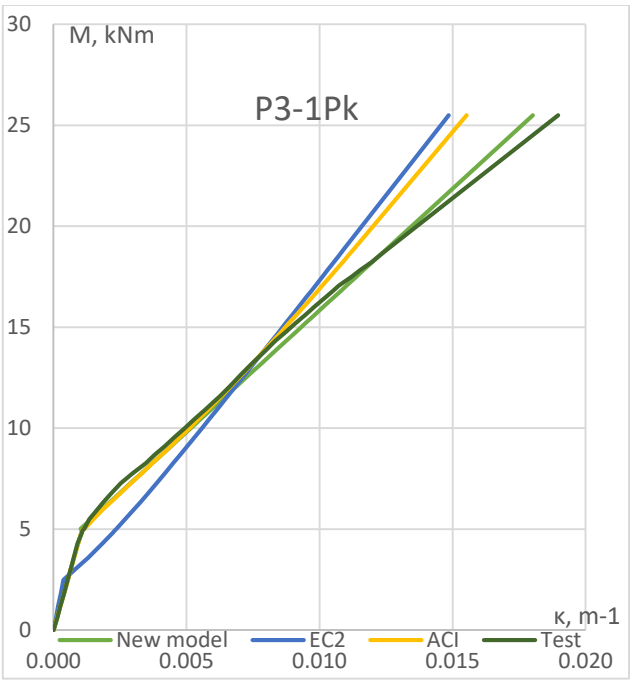

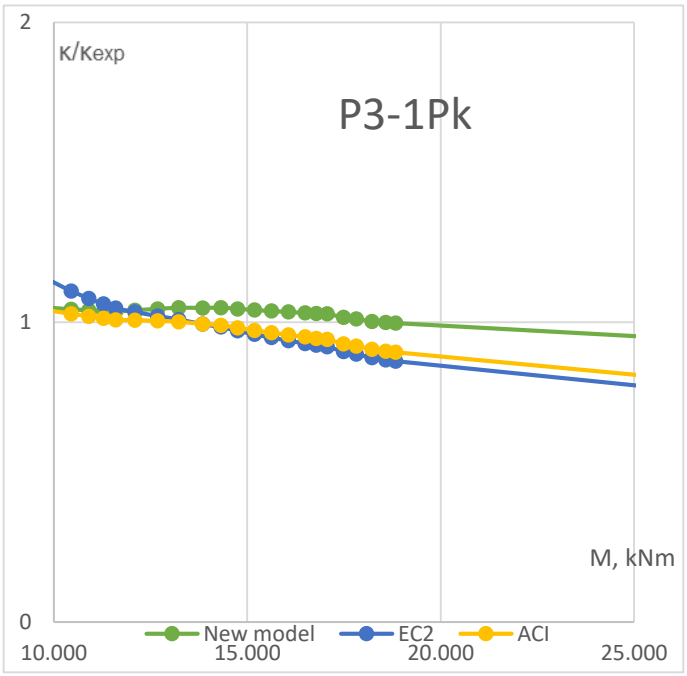

Figure 27:Predicted curvature of test RC beam P3-1PK (Figarovskij 1992)

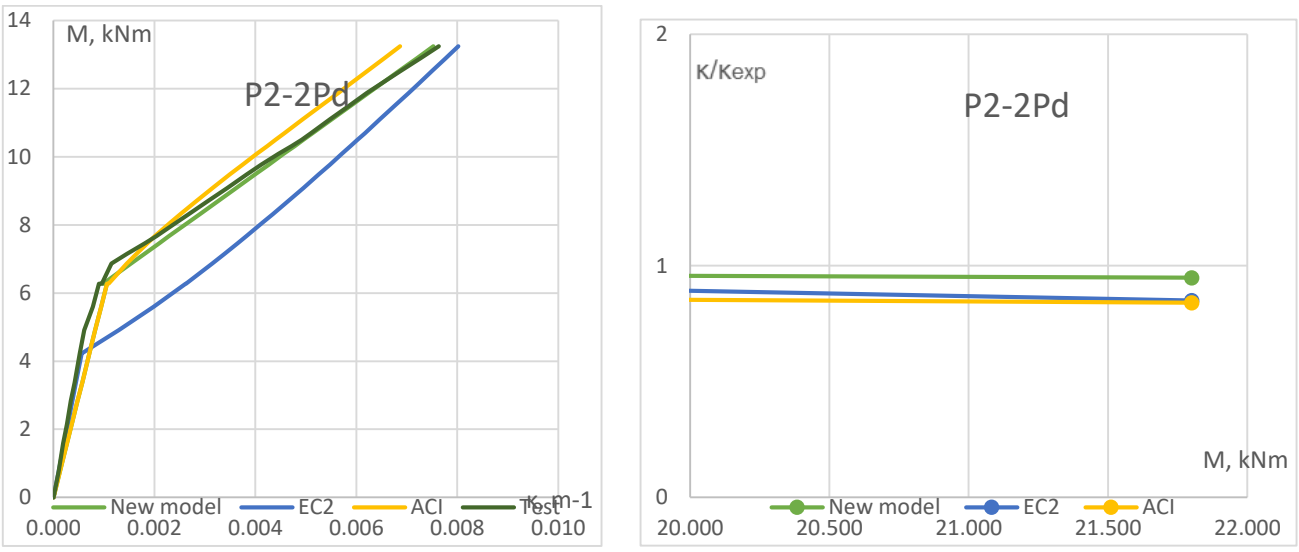

Figure 28:Predicted curvature of test RC beam P2-2Pd (Figarovskij 1992)

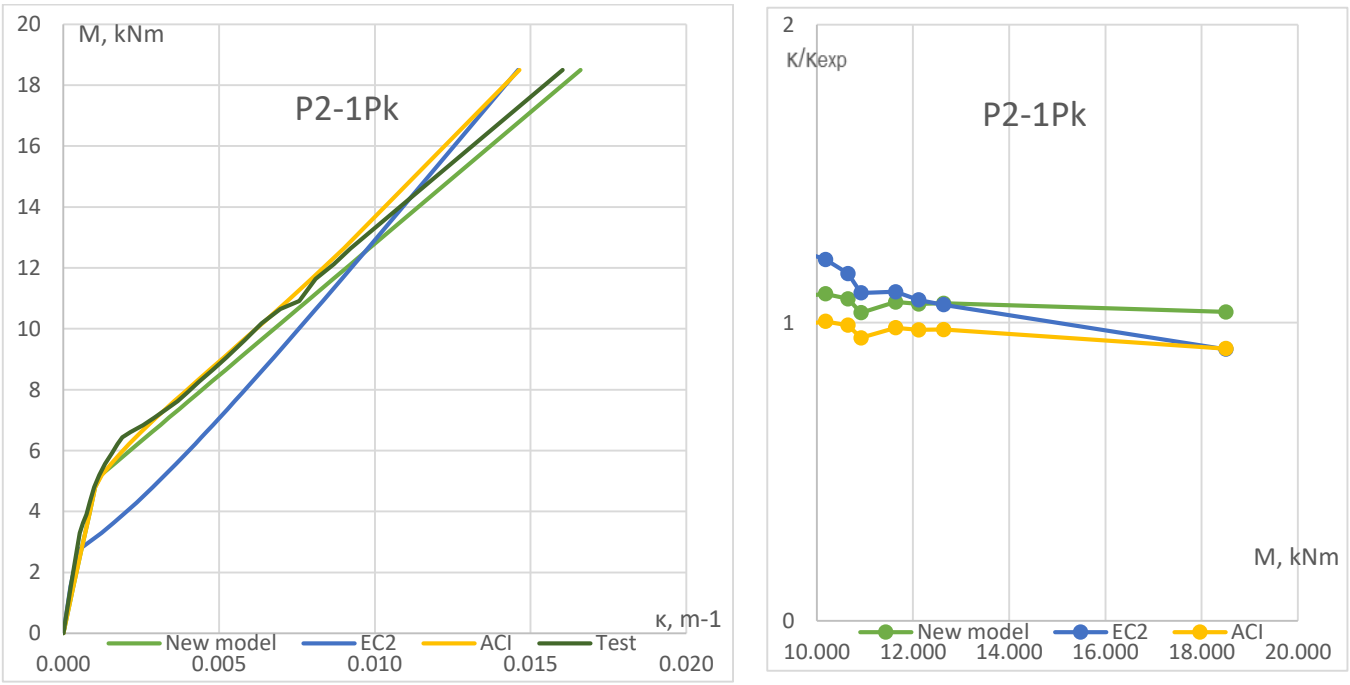

Figure 29:Predicted curvature of test RC beam P2-1PK (Figarovskij 1992)

The following basic statistical results were obtained for each of the theoretical model:

Eurocode Code 2: mean value *m* =1.197; standard deviation s = 0.550; coefficient of variation

v=0.459

Kaklauskas & Sokolov (2024): mean value *m* =0.990; standard deviation s = 0.174; coefficient of variation v= 0.175. The above results are also presented in a tabular form:

Table 6:Statistical results

	GK&AS	***EC2***	***ACI***
Mean	0.990	1.197	0.863
Std. dev	0.174	0.550	0.175
CV	0.175	0.202	0.459

For a limited amount of the test data, it can be concluded that:

The design code methods in many cases given give unsafe predictive results: The mean value for both tand Model Code 2010 techniques is below unity.

The Kaklauskas and Sokolov model is characterized by the mean value 0.990 which closest to unity from the three models. The mean value for the design methods are: 1.197 (EC2) and 863 (ACI)

The Kaklauskas and Sokolov model provides the smallest scatter with the coefficient of variation (0.175) being less than the ones for the ACI (0.202) and the EC2 (0.459).

2.2 DEFLECTION PREDICTIONS OF CONCRETE BEAMS REINFORCED WITH STEEL BARS AND FIBERS (SFRC)

2.2.1 The models employed

The comparative analysis included the following models: RILEM, Model Code 2010, and the Kaklauskas and Sokolov model(2024). These models are briefly described

RILEM

The main part of the RILEM model is the residual tensile strength of SFRC which is described in section 1.5.1. The behaviour of the compressive concrete and tensile reinforcement is taken as linear elastic assuming the respective modulus of elsticity. The moment-curvature behaviour of concrete beams is obtained using a standard software of layer model developed by the team of the supervisor of the MSC project. The main principles of the layer models are descried below.

Model code 2010

The main part of the RILEM model is the residual tensile strength of SFRC which is described in section 2.1.1. The behaviour of the compressive concrete and tensile reinforcement is taken as linear elastic assuming the respective modulus of elsticity. The moment-curvature behaviour of concrete beams is obtained using a standard software of layer model developed by the team of the supervisor of the MSC project. The main principles of the layer models are descried below.

LAYER MODEL

The layer model is employed to calculate moment – curvature diagrams of R/SFRC beams using the residual strength of RILEM and Model Code 2010. Figure 8(a) depicts a non-prestressed, doubly reinforced (fiber) concrete member of I-section. The beam's cross-section is divided into horizontal strata that correspond to concrete or reinforcement. Material qualities may vary across layers, but are believed to remain consistent throughout their thickness.

The corresponding area's condition determines the thickness of the reinforcement layer. For reinforcement material idealization, a linear stress-strain connection has been established. The compressive concrete is assumed to also follow the linear stress-strain relationship.

A computer software, created by the research group of the supervisor of the MSc thesis, can be used to determine the average stress and strain condition at any location on a beam while ignoring shear effects as well as deflections and curvatures. The following stages are used to iteratively perform the computation for a given external moment:

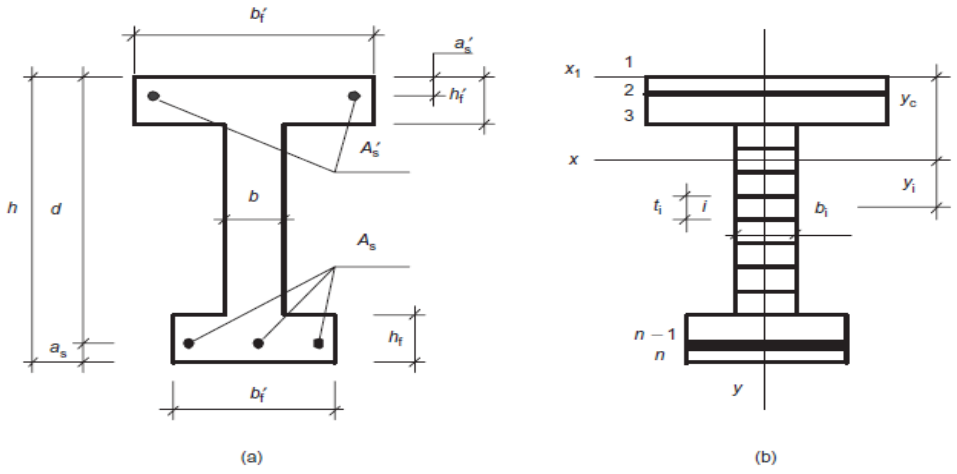

Figure 30:cross-section of doubly reinforced concrete member in layered approach

(a) In the first iteration, elastic material properties are assumed for all the layers.

(b) Geometrical characteristics are calculated for the

transformed cross-section; see Fig. 8(b):

$$A_{\text{tr}} = \sum_{i=1}^{n} b_i t_i \frac{E_i}{E_{\text{c}}}, S_{x1,\text{tr}} = \sum_{i=1}^{n} b_i t_i d_i \frac{E_i}{E_{\text{c}}}$$

$$y_{\text{c}} = \frac{S_{x1,\text{tr}}}{A_{\text{tr}}}, I_{x,\text{tr}} = \sum_{i=1}^{n} \left(\frac{b_i t_i^3}{12} + b_i t_i y_i^2 \right) \frac{E_i}{E_{\text{c}}}$$

where yc is the coordinate of the transformed section with respect to axis x1, and A_{tr} and Sx1,tr are the area and first moment of area of the transformed section, respectively.

yi is the coordinate of the i_{th} layer with respect to the centroid of the transformed cross-section (axis x); bi and ti are the width and thickness of the i_{th} layer (i ¼ 1, 2,..., n) respectively; and Ix,tr is the moment of inertia of the transformed section with respect to axis x.

(c) The expression is used to determine the section's curvature.

$$\kappa = \frac{M}{E_{\text{c}} I_{x,\text{tr}}}$$

The stress σ_i that corresponds to strain ε_i is found for the material diagrams that are assumed. It is established that the secant deformation modulus Ei = σ_i/ε_i.

(d) The longitudinal strain at every layer i is taken as: $\varepsilon_i = \kappa y_i$

(e) For the postulated material diagrams, the stress corresponding to strain is calculated. The secant deformation modulus $E_i = \sigma_i/\varepsilon_i$ is found.

(f) The determined secant deformation modulus Ei is compared to earlier assumptions or computations.

If the agreement for a single layer does not meet the expected error limits, a new iteration begins from step (b).

(g) Once the deformation modulus E_i has converged over all layers, the strains, stresses, and curvature are evaluated. Mohr's integral approach calculates deflection using equivalent computations for additional beam sections.

KAKLAUSKAS and SOKOLOV (2024)

INVERSE TECHNIQUE FOR DEVELOPING A CURVATURE MODEL

The inverse technique for SFRC beams is illustrated. Figure 30 shows that β_0 parameter is related to the fiber volume V_f characteristic.

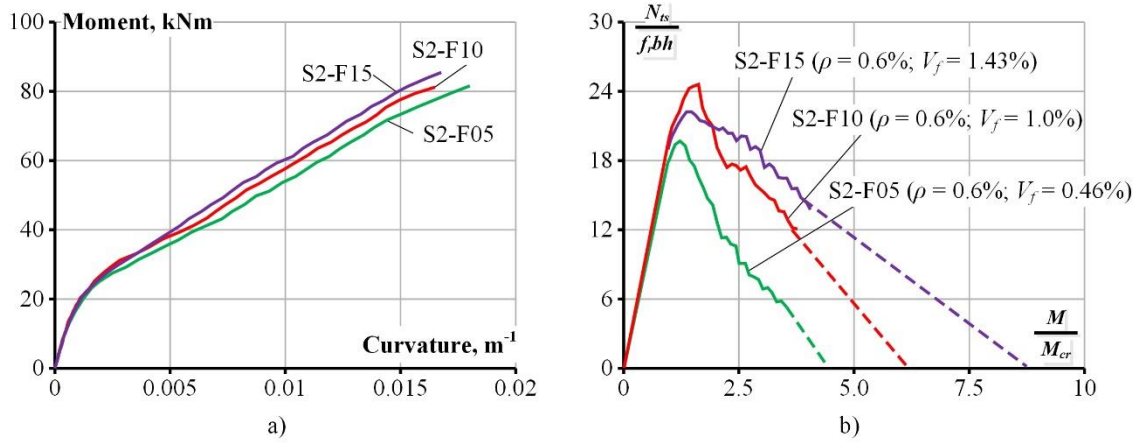

Figure 31: The calculation of resultant tension stiffening force.

A MOMENT-CURVATURE MODEL BY KAKLAUSKAS AND SOKOLOV (2024)

The model uses the following revision of Assumption 3:

Assumption 3: The state of fully cracked section is reached at the bending moment β0Mcr.

The proposed model is illustrated in Fig. 13. The moment – curvature relationship linearly connects two points – 1 and 2, both being easily determined. Point 1 is described by the bending moment Mcr and respective curvature κ1 calculated as for elastic section (see Kaklauskas and Sokolov 2021). At point 2 with bending moment M2=β0 Mcr, curvature κ2 is defined as for the fully cracked RC section. Then curvature is expressed as

$$\kappa = \kappa_1 + (\kappa_2 - \kappa_1)\,(M/M_1 - 1)/(\beta_0 - 1) \tag{1}$$

The dependence of parameter β0 on the volume of fibers, V_f, was obtained empirically based on the test data of 36 R/SFRC beams reported in the literature. The dependence of β_0 on V_f is depicted in Fig. 3b and expressed by this linear formula:

$$\beta_0 = 6.25V_f + 1 \tag{2}$$

In the above formula, V_f is expressed in percent. For small V_f values ($V_f \leq 0.32\%$), β_0 is taken 3 (Fig. 3b) as for the ordinary reinforced concrete members (Kaklauskas and Sokolov 2021).

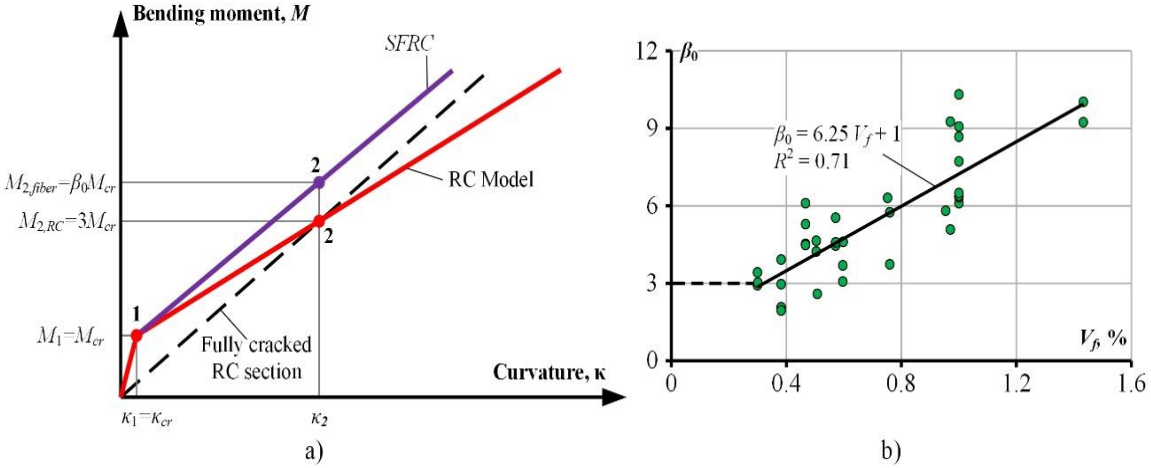

Figure 32: The new curvature mode (Kaklauskas and Sokolov 2024) l: a) moment – curvature relation; b) parameter β0 versus fiber volume

2.2.1 Test data used in the analysis of sfrc beams

Nine SFRC beams having different geometrical and materials characteristics collected from the literature were used to assess the predictive capabilities of the models discussed. Main characteristics of the beams, like section height, effective depth, with, reinforcement area, reinforcement ratio, fiber volume, fiber length and diameter ratio, modulus of elasticity of steel and concrete are presented in Table 6. In total, 52 experimental curvatures points were used in the analysis.

Table 7:Main characteristics of SFRC specimens

Specimen	h	b	d_{sb}	A_{sb}/A_{st} mm²	ρ_{sb}/V_f %	l_f/d_f mm	f_c/f_{sy} MPa	M_{cr}^{ana} kNm
R300RF-F60-1.0	300	200	260	755/57	0.99/1.00	55/1.00	48.2/582	18,2
R300RF-F35-1.0	305	271	215	466/57	0.61/0.46	55/1.00	48.1/632	18,3
R600RF-F35-1.0	306	277	271	477/56	0.61/0.46	55/1.00	55.6/559	20
B-2-F03	250	200	215	477/56	0.62/1.43	55/1.00	52.2/559	19
R150RF-F35-1,0	250	200	215	798/56	1.06/0.46	55/1.00	55.6/564	19,7
S2-F05	300	271	215	798/56	1.05/1.00	55/1.00	47.9/564	18,2
B3-F06	250	200	215	798/56	1.06/1.43	55/1.00	52.2/564	18,9
R150RF-F60-1,0	302	302	252	477/56	0.62/1.00	55/1.00	47.9/559	18,4

2.2.2 Calculated moment curvature digrams and statistical results

The moment – curvature diagrams of the test SFRC beams predicted by the three models are shown in Figures 33 to 40. The figures also show the normalized curvature – bending moment moments graphs.

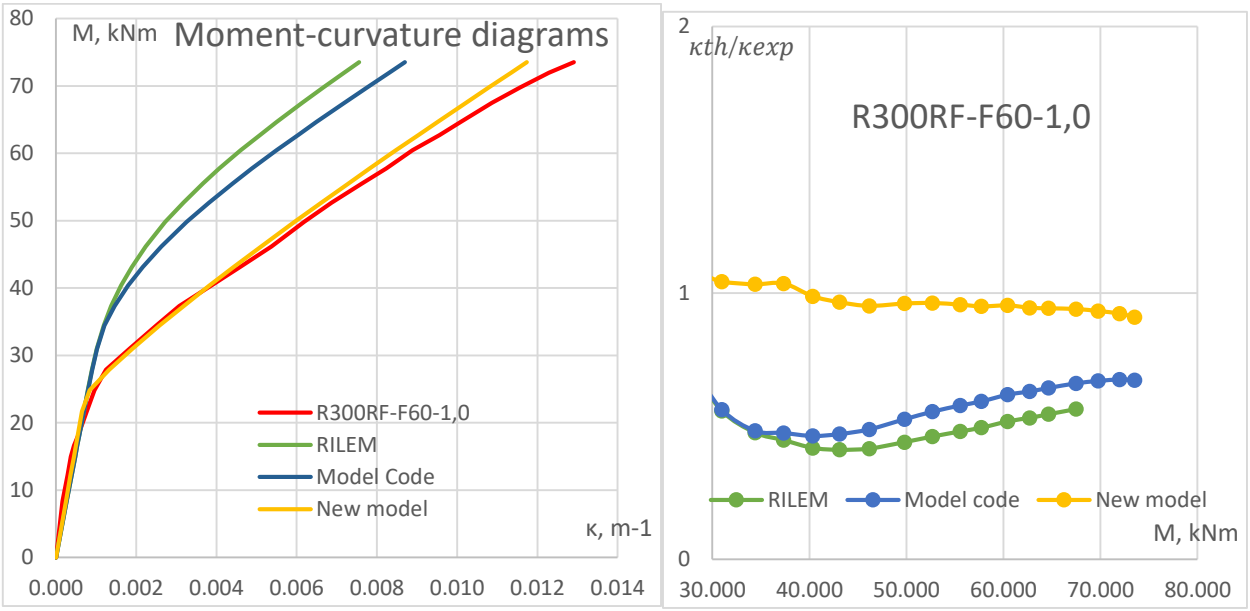

Figure 33:Predicted curvature of test RC beam R300RF-F60-1.0 (Montaignac et. al. 2012)

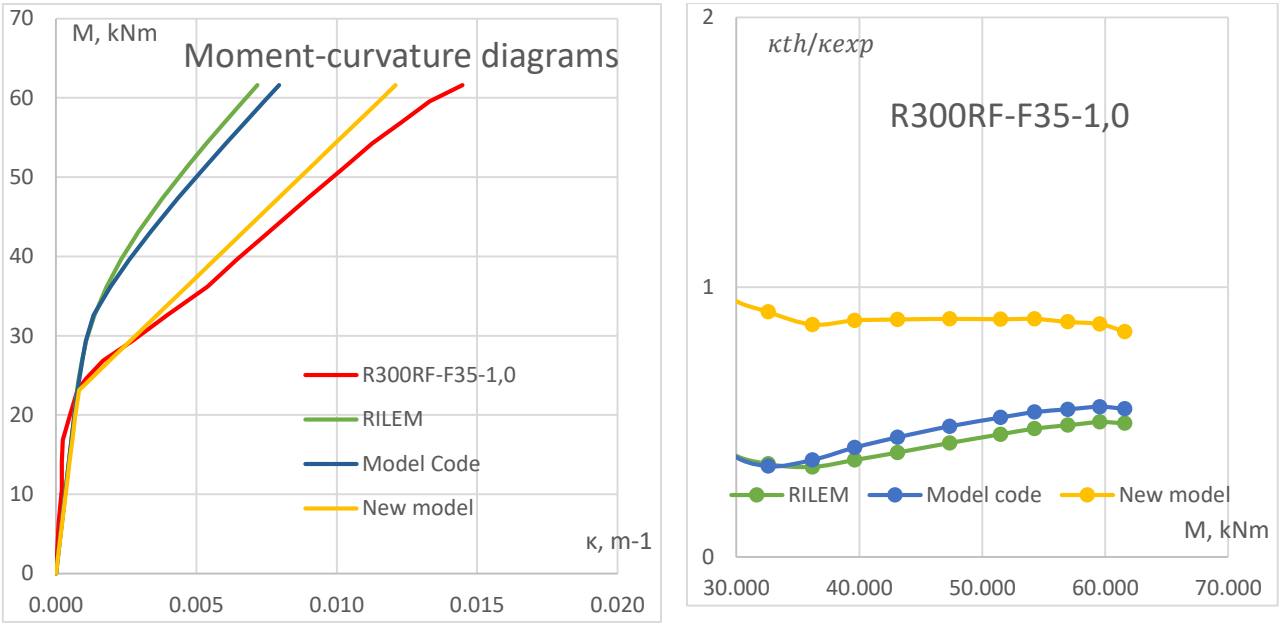

Figure 34:Predicted curvature of test SFRC beam R300RF-F35-1.0(Montaignac et. al. 2012)

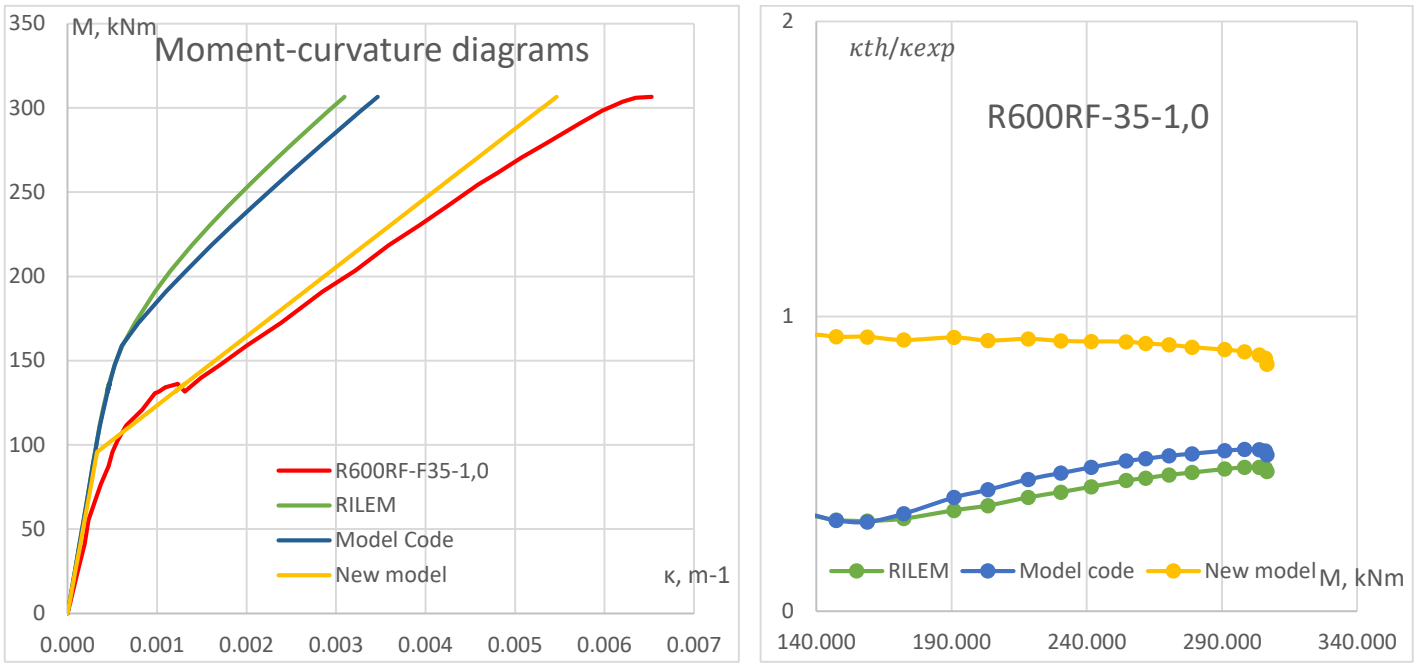

Figure 35:Predicted curvature of test SFRC beam R600RF-1,0(Montaignac et. al. 2012)

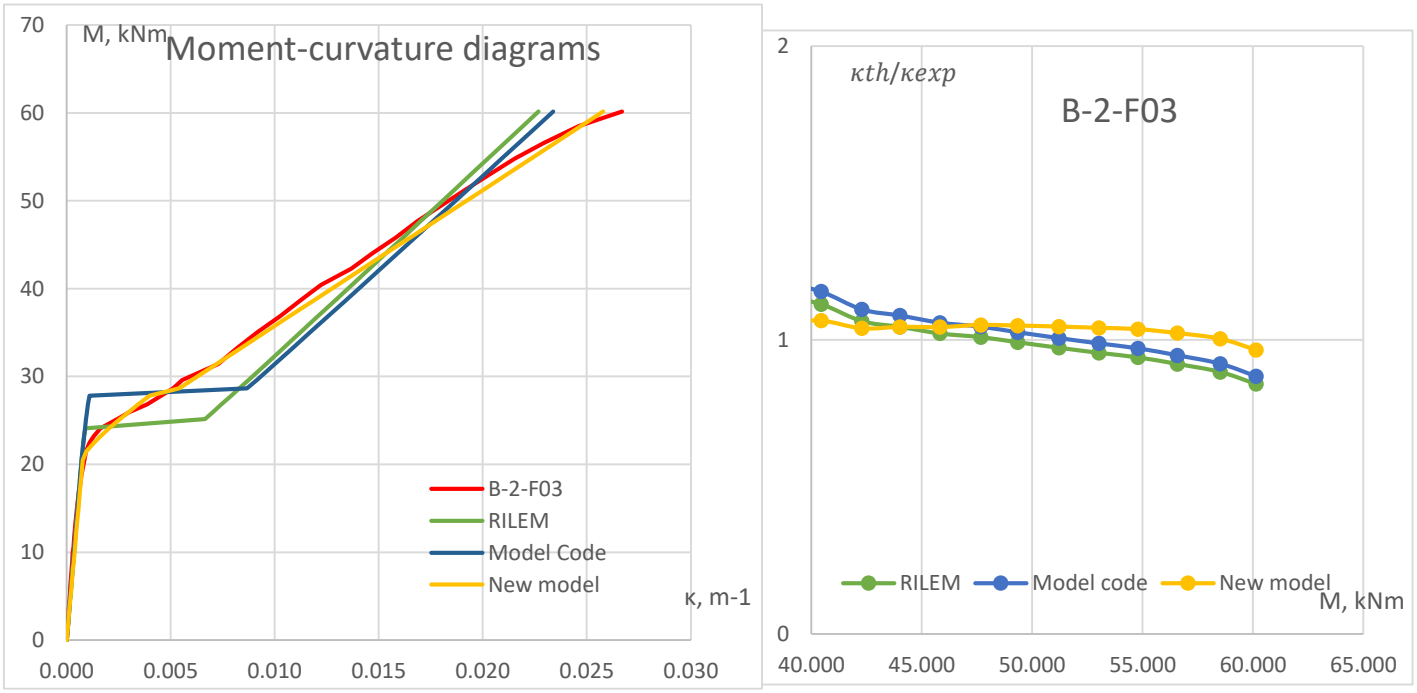

Figure 36:Predicted curvature of test SFRC beam B-2-F03 (VilniusTECH)

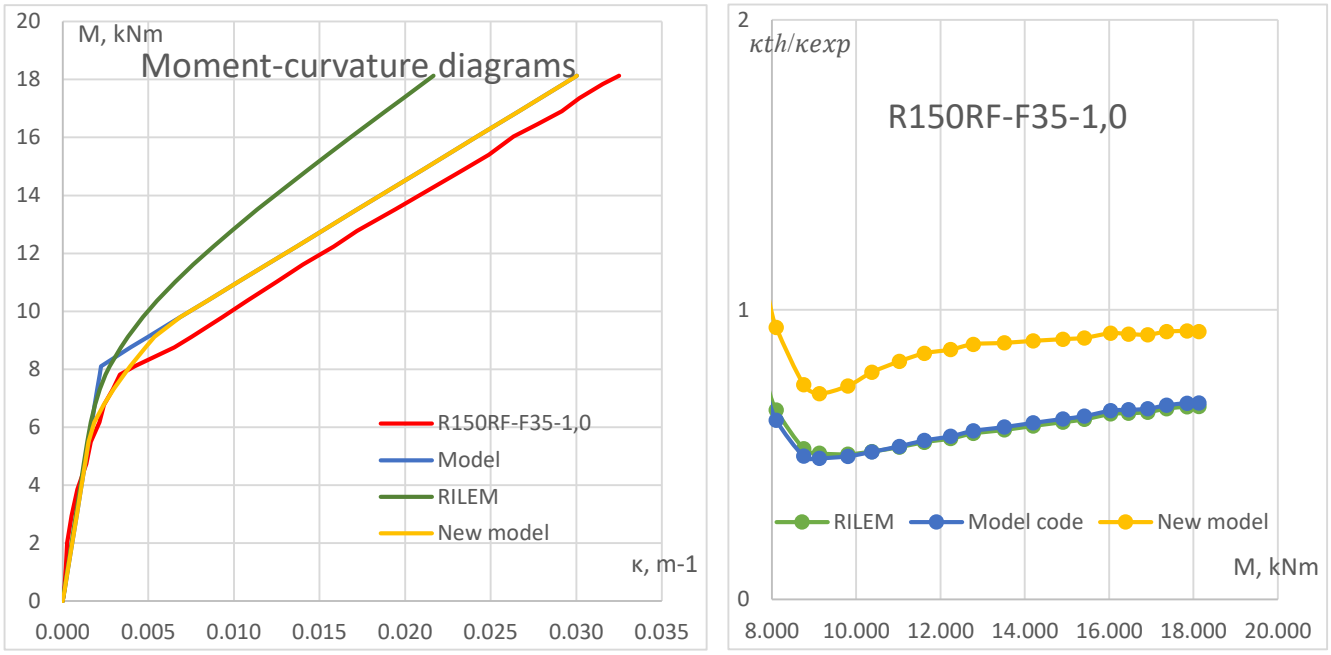

Figure 37:Predicted curvature of test SFRC beam R150RF-F35-1,0(Montaignac et. al. 2012)

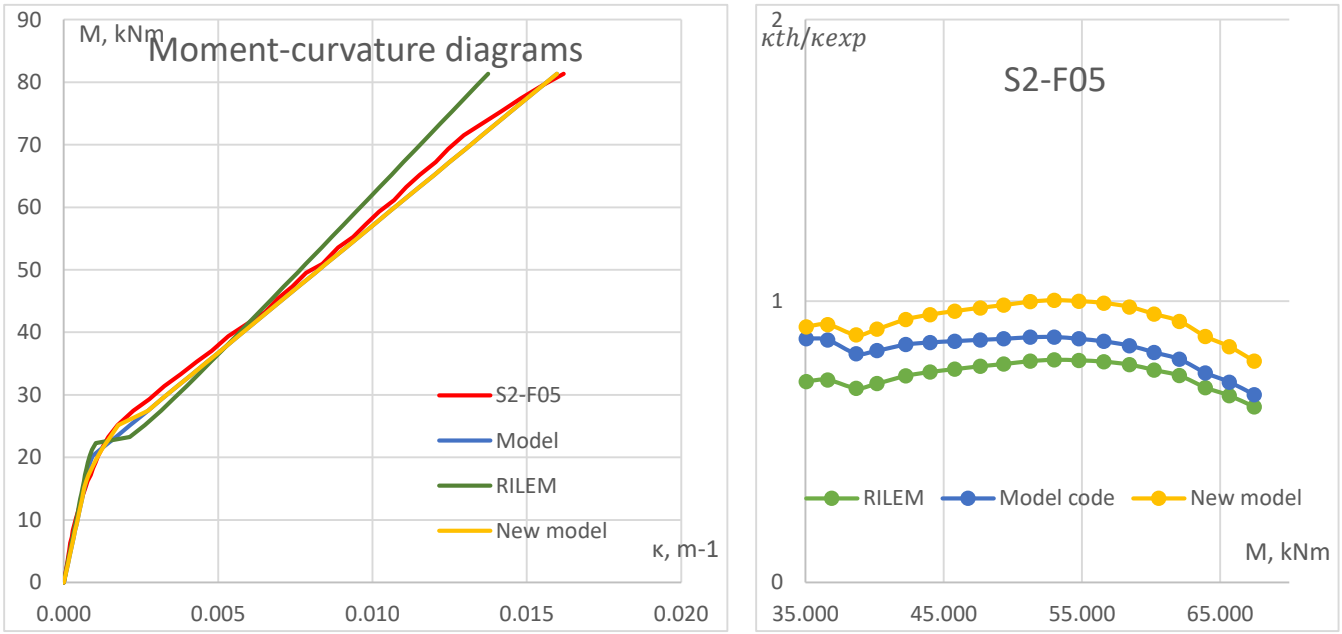

Figure 38:Predicted curvature of test SFRC beam S2-F05(Montaignac et. al. 2012)

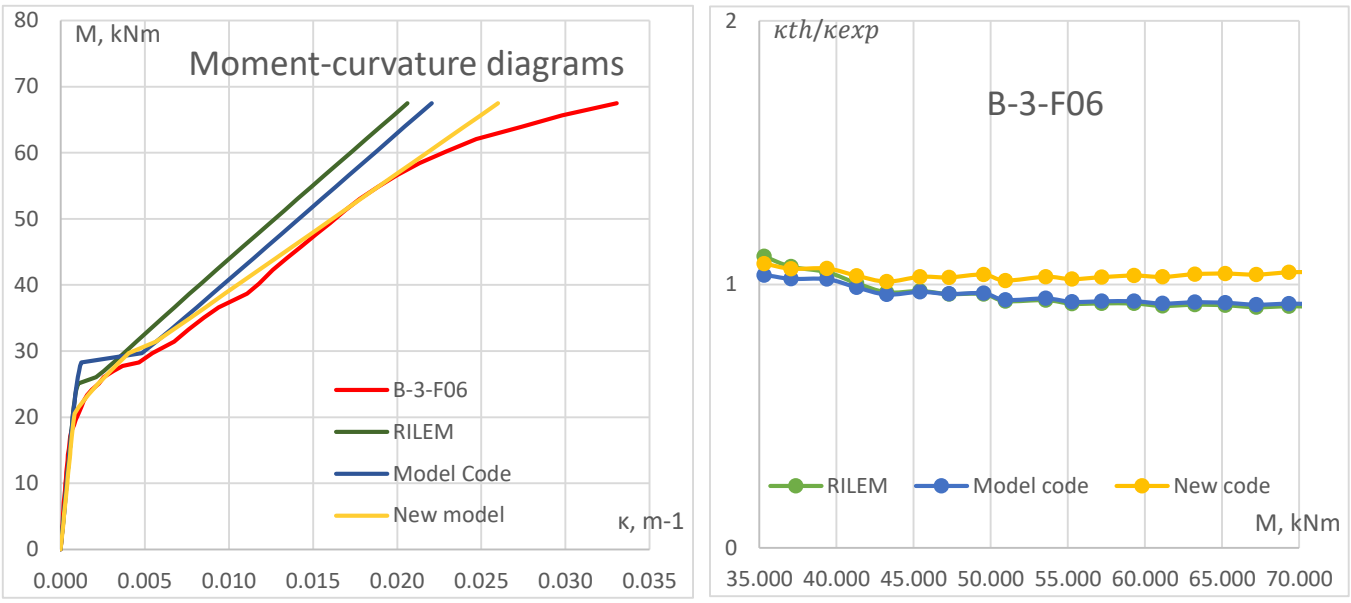

Figure 39:Predicted curvature of test SFRC beam S2-F05(Barros)

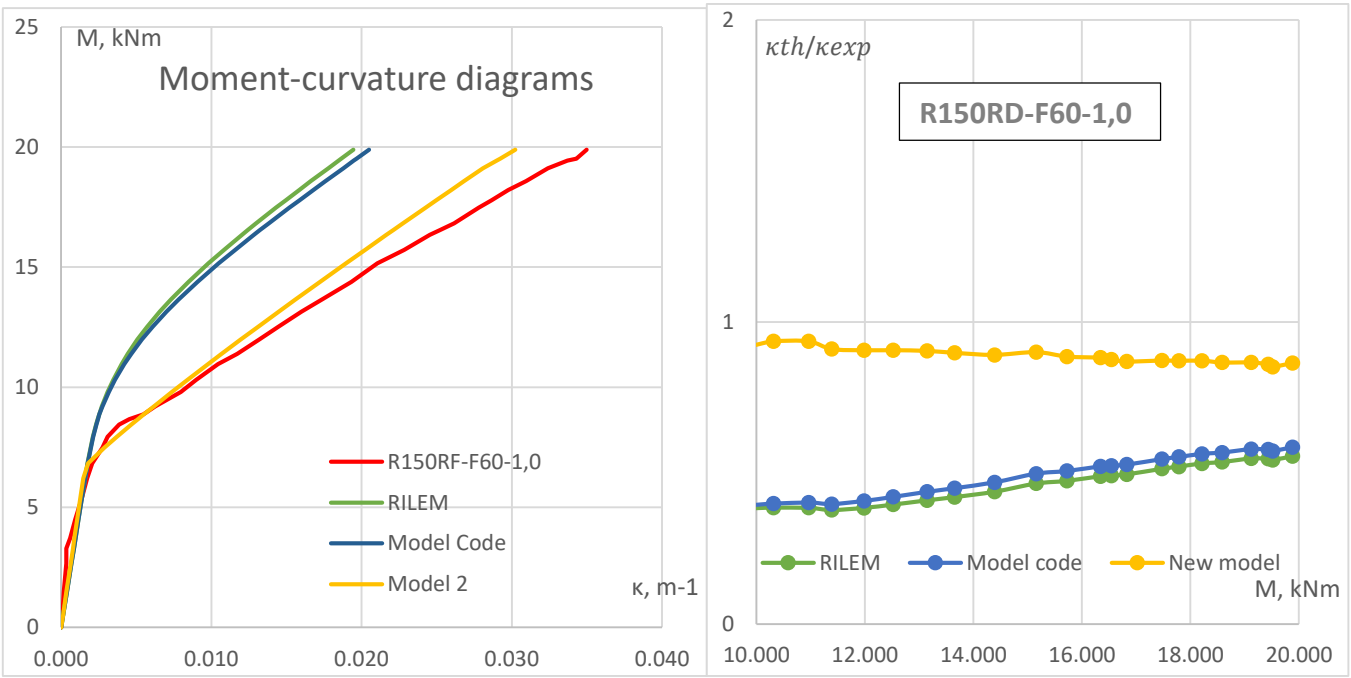

Figure 40:Predicted curvature of test SFRC beam R150RD-F60-1,0 (Montaignac et. al. 2012)

The following basic statistical results were obtained for each of the theoretical model:

RILEM: mean value *m* =0.661; standard deviation s = 0.297; coefficient of variation v= 0.449.

Model Code 2010: mean value *m* =0.641; standard deviation s = 0.247; coefficient of variation v= 0.386.

Kaklauskas & Sokolov (2024): mean value *m* = 0.965; standard deviation s = 0.103; coefficient of variation v= 0.107.

Table 8:Statistical results

	GK&AS	***RILEM***	***MODEL CODE***
Mean	0.965	0.661	0.641
Std. dev	0.103	0.297	0.247
CV	0.107	0.449	0.386

For a limited amount of the test data, it can be concluded that:

The design code methods in many cases given give unsafe predictive results: The mean value for both the RILEM and Model Code 2010 techniques is below unity.

The Kaklauskas and Sokolov model is characterized by the mean value 0.965 which closest to unity from the three models.

The Kaklauskas and Sokolov model provides the smallest scatter with the coefficient of variation (0.107) being less than the ones for the RILEM (0.449) and the Model Code (0.386).

2.2.3 Conclusion of Chapter 2

This chapter evaluates the design codes for short-term curvature of reinforced concrete beams and SFRC beams explores the predictive capability of the new curvature model proposed by Kaklauskas and Sokolov by comparing the calculated instantaneous curvatures with test data on reinforced concrete and SFRC beams. The data set is based on experimental data on mid-span curvatures reported by numerous researchers and contains experimental procedures for 20

reinforced concrete beams and 9 SFRC beams. All specimens were tested in a four-point bending scheme. The comparison to test data was performed for several intervals of stress intensity and included four other models.

3. GENERAL CONCLUSIONS AND RECOMMENDATIONS

1. Most of the current design approaches for steel fiber reinforced concrete (SFRC) elements require the knowledge of the residual strength of (SFRC) in tension with the latter characteristic being obtained from standard bending tests. The involvement of extra tests hampers a wider application of such structures in practice.

2. Recently by Kaklauskas and Sokolov proposed a curvature model for SFRC bending members that does not require the characteristic of the residual strength.

3. The new model for SFRC members is based on the principles of the classical approach, used for RC members, with one assumption revised. This assumption is related to the bending stiffness of the fully cracked section that is clearly perceived by the designers.

4. While the design code methods (e.g. Model Code 2010) use different concepts for the curvature analysis of RC and SFRC members, the model by Kaklauskas and Sokolov is based on a unified concept and basically is the same model for RC and SFRC members with the difference of a single parameter that takes into account the amount of fibers.

5. A limited comparative analysis of curvature predictions for RC beams has shown that

The current study based on a limited amount of test data has shown that that the new model offers a more reliable way to predict curvatures both in RC and SFRC beams compared to the design code technique. The proposed model demonstrated consistent prediction results, with the mean normalized curvature ($\kappa th/\kappa exp$) being close to unity. The new model also showed superiority over design code techniques in terms of the coefficient of variation.

6. Future studies should be dedicated to improving the predictions of crack resistance of the new model.

2.3 REFERENCES

- Sutera, L. (2019). Ottimizza (beton.) (Sons, 2013)zione di un solaio ibrido= Optimization of Hybrid Flat Slab (Doctoral dissertation, Politecnico di Torino).
- Kaklauskas, G., Sokolov, A., & de Barros, J. A. O. (2024). A design methodology for fibre reinforced concrete elements in serviceability conditions integrating tension softening and stiffening effects. *Engineering Structures*, *311*, 118199.
- (Meškėnas A. , 2018). (2018). Serviceability analysis of steel fibre reinforced concrete beams.
- Bischoff, P. H. (2007). Rational model for calculating deflection of reinforced concrete beams and slabs. Canadian Journal of Civil Engineering, 34(8), 992-1002.
- ACI 318-19, 318-19 Building Code Requirements for Structural Concrete and Commentary. American Concrete Institute, 2019. doi: 10.14359/51716937.
- Vandewalle, L., di Prisco, M., & Plizzari, G. (2010). Fiber reinforced concrete in the new FIB Model Code. Codes in Structural Engineering, 2, 1325-1332.
- Löfgren, I. (2005). Fibre-reinforced concrete for industrial construction. Department of civil and environment engineering. Chalmbers university of technology, Göteborg, Sweden.
- Ezeldin & Balaguru 1992, Hsu & Hsu 1994, Someh & Saeki 1994, Mansur *et al.* 1999, Nataraja *et al.* 1999, Bencardino *et al.* 2008, Riz- zuti & Bencardino 2014
- EN, B. (2005). 14651: 2005+ A1: 2007. Test method for metallic fibre concrete–Measuring the flexural tensile strength (limit of proportionality (LOP), residual). British Standards Institution: London, UK.
- Blanco Álvarez, A. (2013). Characterization and modelling of SFRC elements.
- G. Kaklauskas and A. Sokolov, “A peculiar value of M to M raVo: Reconsidering assumpVons of curvature analysis of reinforced concrete beams,” Appl. Eng. Sci., vol. 7, p. 100053, Sep. 2021, doi: 10.1016/j.apples.2021.100053.
- Shah, S. P., Daniel, J. I., Ahmad, S. H., Arockiasamy, M., Balaguru, P. N., Ball, C. G., & Zollo, R. F. (1993). Guide for specifying, proportioning, mixing, placing, and finishing steel fiber reinforced concrete. ACI Materials Journal, 90(1), 94-101
- Soranakom, C., & Mobasher, B. (2009). Flexural design of fiber-reinforced concrete. ACI Materials Journal, 106(5), 461.

- Code, C. F. M. (1993). Comité euro-international du béton. Bulletin d'information, 213(214), 787
- Blanco, A., Pujadas, P., De la Fuente, A., Cavalaro, S., & Aguado, A. (2013). Application of constitutive models in European codes to RC–FRC. Construction and Building Materials, 40, 246-259
- ACI Committee, 3. (2008). Building code requirements for structural concrete (ACI 318-08) and commentary. American Concrete Institute.
- Clark, Leslie Arthur, and D. M. Speirs. Tension stiffening in reinforced concrete beams and slabs under short-term load. No. 42.521 Tech Rpt.. 1978.
- (Figarovskij, 1992)Figarovskij, V. V. Experimental investigation of stiffness and cracking of reinforced concrete flexural members subjected to short-term and long-term loading. Diss. PhD dissertation. Moscow: NIIZhB. 210 p.(In Russian), 1962
- Barros Arana, Diego. "Historia general de Chile I." (2021).
- C.-K. Choi and S.-H. Cheung, "Tension stiffening model for planar reinforced concrete members," Comput. Struct., vol. 59, no. 1, pp. 179–190, Apr. 1996, doi: 10.1016/0045-7949(95)00146-8.
- V. Gribniak, V. Cervenka, and G. Kaklauskas, "Deflection prediction of reinforced concrete beams by design codes and computer simulation," Eng. Struct., vol. 56, pp. 2175–2186, Nov. 2013, doi: 10.1016/j.engstruct.2013.08.045
- P. H. Bischoff, "Reevaluation of Deflection Prediction for Concrete Beams Reinforced with Steel and Fiber Reinforced Polymer Bars," J Struct Eng, vol. 131, no. 5, pp. 752–767, May 2005, doi: 10.1061/(ASCE)0733-9445(2005)131:5(752).
- G. W. Washa and P. Fluck, "Effect of compressive reinforcement on the plastic flow of reinforced concrete beams," presented at the Journal Proceedings, 1952, pp. 89–108
- R. Ian Gilbert, "Deflection Calculation for Reinforced Concrete Structures—Why We Sometimes Get It Wrong," SJ, vol. 96, no. 6, pp. 1027–1032, 1999, doi: 10.14359/779.